

Student Research Project

SPECTROSCOPIC ELLIPSOMETRY FOR THE IN-SITU INVESTIGATION OF ATOMIC LAYER DEPOSITIONS

Varun Sharma



Student Research Project

SPECTROSCOPIC ELLIPSOMETRY FOR THE IN-SITU INVESTIGATION OF ATOMIC LAYER DEPOSITIONS

Submitted by:

Varun Sharma

born on March 24, 1988, in Ferozepur, India

Matriculation number: 3834614

Supervised by:

Dipl.-Ing. Marcel Junige

Dipl.-Ing. Martin Knaut

Responsible Professor:

Prof. Dr. rer. nat. Johann W. Bartha

Submitted on:

Dresden, April 30, 2014



TASK FORMULATION FOR A STUDENT RESEARCH PROJECT

Student's name: Varun S H A R M A born on March 24, 1988

Subject:

»Spectroscopic ellipsometry for the in-situ investigation of atomic layer depositions«

Spectroscopic ellipsometry (SE) is a non-invasive measurement technique, which is fast, accurate, self-referencing, and highly sensitive to the smallest change on a solid-state surface. Thus, SE is ideally suited for the in-situ characterization of a material's deposition, modifying an investigated sample from its initial stage towards a film covered surface.

Atomic layer deposition (ALD) is a special kind of chemical vapor deposition, which is mainly characterized by a self-terminating surface coverage in the progress of the two distinctive reaction steps. As a result, ALD enables a highly conformal coating of complex three-dimensional-shaped surfaces including a unique film thickness control in the sub-nanometer range. The ALD of aluminum oxide (Al_2O_3) can be regarded as a standard model process.

Objectives: As a result of the student research project, the capability of in situ SE is to be demonstrated with respect to a detailed characterization of the Al_2O_3 ALD model process, comprising a comprehensive study of various process parameter interdependencies. Consequently, a reliable process for the Al_2O_3 ALD has to be developed from trimethylaluminum (TMA) and ozone (O_3). The ALD characteristics of the TMA/ O_3 process should be compared, applying two different gas distribution plates in the gas shower head.

Sub-tasks:

1. Surveying the literature in comparison of the TMA/water with the TMA/ O_3 process
2. Planning of experiments
3. Familiarizing with the FHR ALD 300 tool, including the in situ ellipsometer as well as a selection of direct surface analysis techniques for referencing purposes
4. Conducting and minuting the planned experiments;
evaluating the acquired ellipsometric spectra as well as referencing measurements
5. Interpreting, formulating and discussing the received results in writing

Supervisors: Dipl.-Ing. Marcel Junige; Dipl.-Ing. Martin Knaut

Handed over on: October 16, 2012

SELF DECLARATION

I hereby declare, that I have completed and submitted my student research project on 'Spectroscopic Ellipsometry for the in-situ investigation of Atomic Layer Depositions' on this day. I also declare that this project report was independently written by me. And I have used no resources and quotations other than those specified in this report.

Dresden, April 30, 2014

Varun Sharma

CONTENTS

Lists of Abbreviations and Symbols	XII
Lists of Figures and Tables	XVIII
1 Introduction	1
I Theoretical Part	3
2 Alumina in electronic industry	5
3 Atomic Layer Deposition	7
3.1 History	8
3.2 Process definition	8
3.3 Benefits and limitations	8
3.4 ALD growth mechanism of Aluminium oxide from TMA/O ₃	9
3.5 Growth kinetics	12
3.6 Comparison of TMA/O ₃ and TMA/H ₂ O – A literature survey	14
4 Spectroscopic Ellipsometry	17
4.1 Introduction	18
4.2 Measuring Principle	18
4.3 Fitting and models	20
4.4 Advantages and limitations	22
5 X-Ray Photoelectron Spectroscopy	25
5.1 Introduction	26
5.2 XPS mechanism	26
5.3 XPS analysis	26
5.4 Advantages and limitations	27
6 Atomic Force Microscopy	29

II	Experimental Part	31
7	Methodologies	33
7.1	Experimental setup	34
7.2	ALD process	36
7.3	Experiment design	36
7.4	Spectroscopic Ellipsometry	38
7.4.1	Tool and software	38
7.4.2	Data acquisition	38
7.4.3	Data evaluation	40
7.4.4	Post processing of data	41
7.4.5	Sources of errors in SE	43
8	Results and discussion	47
8.1	Introduction	48
8.2	Kinetic ALD characteristic curves	48
8.2.1	TMA exposure	49
8.2.2	Argon purging after TMA exposure	50
8.2.3	Ozone exposure	51
8.2.4	Argon purging after ozone exposure	52
8.3	Impact of process parameters on characteristic ALD growth attributes and film properties	53
8.3.1	Total process pressure	53
8.3.2	Ozone flow	54
8.3.3	Deposition temperature	56
8.4	Reproducibility	61
9	Conclusions and outlook	63

References	68
III Appendix	77
A Reference temperatures and ozone flow	79
B Process parameters	81

LISTS OF ABBREVIATIONS AND SYMBOLS

LIST OF ABBREVIATIONS

AFM	atomic force microscopy
Al ₂ O ₃	aluminium oxide also alumina
ALD	atomic layer deposition
AOI	angle of incidence
CH ₃	methyl ligands
c-Si	crystalline silicon
CVD	chemical vapor deposition
DRAM	dynamic Random Access memory
e.m.	electro magnetic
ESCA	electron spectroscopy for chemical analysis
Ge	germanium
<i>GPC</i>	growth per cycle
H ₂ O	water
HR	high resolution
ITRS	international technology roadmap for semiconductors
JJ	josephson junction
<i>L_{rem}</i>	ligand removal
MBE	molecular beam epitaxy
MFC	mass flow controller
MIM	metal-insulator-metal
ML	monolayer
MOSFET	metal oxide semiconductor field effect transistor
MRAM	magnetic random access memory
MSE	mean squared error
MTJ	magnetic tunnel junction
NaCl	sodium chloride
natOx	native oxide; ≈ 2 nm SiO ₂
OH	hydroxyl
OLS	optical layer stack

PCB	printed circuit boards
PE	plasma-enhanced
PVD	physical vapor deposition
Q-bit	quantum-bits
QCM	quartz crystal microbalance
<i>RAE</i>	rotating analyser ellipsometer
<i>RCE</i>	rotating compensator ellipsometer
SD	standard deviation
SE	spectroscopic ellipsometry
Si	silicon
Si ₃ N ₄	silicon nitride
SiO ₂	silicon dioxide
SIS	semiconductor-insulator-semiconductor
TMA	trimethylaluminum
<i>M_{ads}</i>	TMA adsorption
UHV	ultra high vacuum; $P \leq 10^{-7}$ Pa
UPS	ultraviolet photoelectron spectroscopy
UV	ultraviolet
Xe	xenon
XPS	x-ray photoelectron spectroscopy

LIST OF SYMBOLS

Constants

- ϵ_0 absolute permittivity
- h PLANCK's constant;
 $h = 4,13566733 \cdot 10^{-15}$ eV s

Greek Symbols

- α absorption coefficient
- θ angle of incidence
- θ_B brewster angle
- Δ phase difference
- ϵ_r real part of complex dielectric function,
also: relative permittivity
- κ extinction coefficient
- ν light frequency
- ϕ work function
- Ψ amplitude ratio
- ρ complex reflectance ratio
- $\vartheta_{\text{Surface}}$ surface temperature
- $\vartheta_{\text{Substrate}}$ substrate temperature
- ϑ_{TMA} TMA-*bubbler* temperature

Symbols

- E_b binding energy
- E_k kinetic energy
- K_{O_3} growth kinetics for ozone exposure
- K_{TMA} growth kinetics for TMA adsorption
- N_{cycle} total number of cycles
- n refractive index
- t_{Ar1} Ar pulse time after TMA exposure

t_{Ar2}	Ar pulse time after O ₃ exposure
t_{O3}	O ₃ exposure time
$T_{thickness}$	total thickness
t_{TMA}	TMA exposure time
t_{cycle}	complete ALD cycle time

Units

A	Ampere
Å	Ångström
°C	Degree Celsius; 0 °C = 273,15 K
eV	Electron Volt; 1 eV = 1 e · 1 V
K	Kelvin
kg	Kilogram
m	Meter
um	Micrometer or Micron
min	Minute
Pa	Pascal
s	Second
sccm	Standard Cubic Centimeter per Minute
THz	Tera-Hertz
V	Volt; 1 V = 1 kg m ² /A s ³
W	Watts, a unit of electrical power

LISTS OF FIGURES AND TABLES

LIST OF FIGURES

3.4.1 Schematic illustration of an ALD cycle	10
3.5.1 complete ALD cycle averaged over 10 ALD cycles	12
4.2.1 Schematic illustration of experimental setups of spectroscopic ellipsometry. Linearly polarized light is incident to a sample substrate with incident angle of θ . The ellipsometry parameters Ψ and Δ , which represent the ratio of amplitudes of s- and p-polarized components of the incident light and the phase difference between them, respectively[Fujiwara 2007, p.82]	19
4.3.1 Schematic representation of a simple optical layered model with two films, parameterized by thickness (t_1, t_2) and optical constants(n, k) [adapted from J.A. Woollam Co. 2011, p.3-43]	20
4.3.2 characterization of physical properties by spectroscopic ellipsometry [adapted from Fujiwara 2007, p.4]	21
5.2.1 Diagram of photoelectric effect in XPS	27
7.1.1 Comparison of Type I (a) and Type II (b) shower head designs	34
7.1.2 Schematic diagram of ALD-300 chamber from FHR Analgenbau GmbH with surface characterization and analysis system from Omicron Nanotechnology GmbH	35
7.4.1 course of the optical layer thickness as revealed by iSE time-discrete data acquisition over the Al_2O_3 ALD cycle number	39
7.4.2 Time-discrete and time-continuous iSE measurements for shower head design of type II	40
7.4.3 optical stack layer model for Al_2O_3 on Si substrate with native oxide	41
7.4.4 actual temperature versus target substrate temperature	41
7.4.5 Schematic representation of 10 ALD cycles	42
7.4.6 signal intensity of 250nm wavelength (red) and optical layer thickness (black) versus ALD process time	44
8.2.1 kinetic ALD characteristic curves for shower head design type I and II at deposition temperature of 150°C and total process pressure of 150 Pa	48
8.2.2 variation in TMA exposure time	49

8.2.3	variation in Ar purging time after TMA exposure	50
8.2.4	variation in O ₃ exposure for both type of shower head designs - a time- continuous irtSE measurement	51
8.2.5	variation in Ar purging time after ozone exposure	52
8.3.1	variation in total process pressure	53
8.3.2	variation in O ₃ flow	54
8.3.3	variation in deposition temperature	56
8.3.4	XPS analysis at different deposition temperature	58
8.3.5	effect of temperature on surface roughness	59
8.3.6	AFM topography after 100 Al ₂ O ₃ ALD cycles at different temperatures . . .	60
8.4.1	reproduced ALD cycle curves	61

LIST OF TABLES

- A.1 actual substrate temperatures corresponding to set-point temperatures . . . 80
- A.2 O₂ and O₃ gas flows with their corresponding needle valve positions 80

- B.1 process parameter variations 82
- B.2 variations in TMA exposure time 82
- B.3 variations in Ar purge time after TMA exposure 83
- B.4 variations in O₃ exposure time 83
- B.5 variations in Ar purge time after O₃ exposure 83

1 INTRODUCTION

Atomic Layer Deposition (ALD) is a special type of Chemical Vapor Deposition (CVD) technique based on self-terminating sequential gas reactions for a conformal and precise growth down to few nanometers range. Ideally due to the self-terminating reactions, ALD is a surface-controlled process, where process parameters other than the choice of precursors, substrates, and deposition temperature have little or no influence [Puurunen 2005 P. 121301-22]. In spite of the numerous applications of growth by ALD, many chemical and physical processes that control ALD growth are not yet sufficiently understood [Jaebum 2002 P.733].

Aim of this student research project is to develop an Aluminium Oxide (Al_2O_3) ALD process from trimethylaluminum (TMA) and Ozone in comparison of two shower head designs. Then studying the detailed characteristics of Al_2O_3 ALD process using various measurement techniques such as Spectroscopic Ellipsometry (SE), x-ray photoelectron spectroscopy (XPS), atomic force microscopy (AFM). The real-time ALD growth was studied by in-situ SE. In-situ SE is very promising technique that allows the time-continuous as well as time-discrete measurement of the actual growth over an ALD process time. The following ALD process parameters were varied and their inter-dependencies were studied in detail: exposure times of precursor and co-reactant as well as Argon purge times, the deposition temperature, total process pressure, flow dynamics of two different shower head designs. The effect of varying these ALD process parameters was studied by looking upon ALD cycle attributes. Various ALD cycle attributes are: TMA molecule adsorption (M_{ads}), Ligand removal (L_{rem}), growth kinetics (K_{O_3}) and growth per cycle (GPC).

I THEORETICAL PART

2 ALUMINA IN ELECTRONIC INDUSTRY

Al_2O_3 is the most common form of Aluminum oxides that occur naturally in its crystalline polymorphic phase $\alpha\text{-Al}_2\text{O}_3$ known as corundum. Al_2O_3 has relatively high melting of 2,345 K. It is resistant to attack by many chemicals and gases. It is also a good electrical insulator but has a very good thermal conductivity [Patnaik 2003, p.11]. Al_2O_3 is widely accepted in many industries like Power Electronics, Optics, Semiconductor, Mechanical, Memories and Computing. In thin film technology Al_2O_3 is deposited in its amorphous phase.

Al_2O_3 is a very important material in high performance electronics [Perrella 2004, p.2]. Al_2O_3 is used in various fields of microelectronic industry. It is used as a gate-oxide in transistors, dielectric in dynamic Random Access memory (DRAM), fast computing applications and in making passive components.

Moreover, at 1 nm thick SiO_2 the leakage current becomes unacceptable therefore there was a strict need to substitute SiO_2 by high-k and metal oxides according to ITRS road map to follow the current Moore's law [Manchanda u. a. 2001, p.351]. Al_2O_3 comes under high-k category which makes it suitable for gate dielectric in metal oxide semiconductor field effect transistors (MOSFETs).

The development of dynamic Random Access memory (DRAM) capacitor dielectrics has been similar to that of gate dielectrics. The idea behind this is to use Al_2O_3 in electronic industry as semiconductor-insulator-semiconductor (SIS) and metal-insulator-metal (MIM) capacitances. Capacitance can be defined as $C = \epsilon_r \epsilon_0 A/d$ and this can be increased by using high-k values, rest are constants for particular geometry [Yeong Kwan Kim u. a., p.370]. The ϵ_r value for Al_2O_3 is 10 (for vacuum $\epsilon_r = 1$) which is approximately 2.5 times higher than conventional Silicon oxide [Jakschik u. a. 2003, p.353].

It is also used as an insulator in magnetic tunnel junctions (MTJs) used for magnetic random access memory (MRAM) which may allow the fabrication of solid state Q-bits based on Josephson junctions (JJs) [Mizuguchi u. a. 2005, P.1] [Zhu u. Park 2006, P.36]. To achieve high performance computing, silicon oxide was replaced by many high-k dielectrics like Al_2O_3 [Manchanda u. a. 2001, p.351]. According to the property of Josephson junctions to perform switching at very high speed of few THz which can be used in high performance computing [Hasuo 1992, p.21] and fast switching memories [H. Suzuki u. a. 1989, p.783].

Al_2O_3 is used as a passivation layer on silicon, the ceramic form is often used as a carrier for thick and thin film passive components and for other small printed circuit boards (PCB). It has relatively low production cost that is combined with its high thermal conductivity [Bernardi u. a. 2004, p.475]

3 ATOMIC LAYER DEPOSITION

3.1 HISTORY

ALD principle was first published under name "Molecular Layering" in the early 1960s by Prof. S.I. Koltsov from Leningrad Technological Institute. The concept of the ALD process was first proposed by Prof. V.B. Aleskovskii in his Ph.D. thesis published in 1952 [Puurunen 2005]. It was the work of Dr. Tuomo Suntola and coworkers in Finland in mid-1970s that made a scientific idea a true thin film deposition technology and later on adopted by an industrial use. Since then it is widely used in manufacturing industries as well as research institute [Nalwa 2002].

3.2 PROCESS DEFINITION

ALD is one of the thin film deposition technique that is based on sequential use of self-terminating surface reactions [Puurunen 2005, p. 121301 - 3]. A material of desired thickness can be grown with ALD by repeating the following characteristic four pulses:

1. Exposure of the first precursor, typically an metal-organic compound (such as TMA).
2. Purge or evacuation of the reaction chamber to remove the non-reacted precursor molecules and the gaseous reaction by-products.
3. Exposure of the second co-reactant (such as Ozone) or another treatment, to activate the surface again for the reaction of the first precursor.
4. Purge or evacuation of the reaction chamber [Puurunen 2005, p. 121301 - 3]

Ideally, each reaction cycle adds a monolayer (ML) of material to the surface, referred to as the growth per cycle GPC. But practically it is not the case: Most ALD processes do not fulfill these criteria [Puurunen 2005, p. 121301 - 38]. Figure 3.4.1 shows a pictorial representation of detailed ALD process and how the depositions occur and reactant by products leave the surface.

3.3 BENEFITS AND LIMITATIONS

In ALD, the thickness of grown material can be controlled very precisely because in the ideal case the film thickness depends only on the number of reaction cycles. Depositions done with an ALD has a better step coverage and side wall deposition. ALD technique is capable to grow very thin films and film properties can be reproduced. ALD

allows high density, low defect density and conformal coatings. Practically, the physical state of films like amorphous and crystallinity can be controlled by varying the process parameters like substrate temperature [cambridge nanotech July].

ALD gives a choice to grow heterogeneous, graded index and doped layers of different materials. Due to availability of various precursors in the market, it is possible to grow almost all materials used in semiconductor industry [Nalwa 2002, p. 116 - 119] [Puurunen 2005].

Other ALD techniques like spatial ALD, roll-to-roll and batch processing can be incorporated to achieve high throughput of wafers per minute. Thus several wafers can be deposited with very fine thin films of different materials [Nalwa 2002, p.108]. Also, in combination of PE-ALD and Flash-ALD, depositions at lower temperature can be achieved esp. for substrates like polymers. Films grown with the help of ALD can be of low stress due to molecular self-assembly.

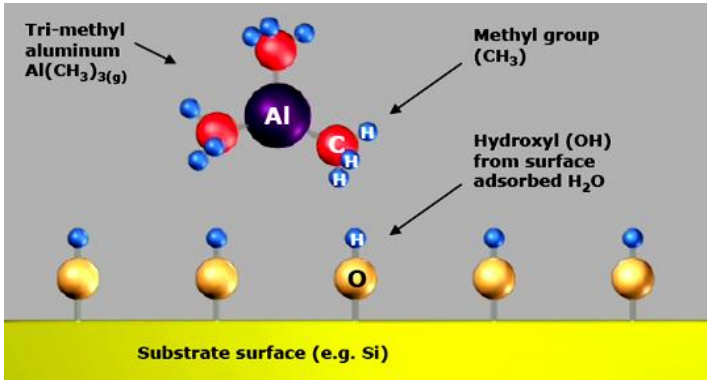
The major limitation of ALD is that it is time consuming as compared to other widely used deposition techniques like physical vapor deposition (PVD), CVD and molecular beam epitaxy (MBE). Although we have wide range of materials available that can be grown by ALD, many important materials like Si, Ge, Si_3N_4 , several multi-component oxides, certain metals cannot currently be deposited by ALD in a cost-effective way [Ritala 2002 p.108]. ALD is technique based on chemical reactions that occur on the surface of substrate, thus there is always a risk of residues being left from the precursors specially carbon or hydrogen.

3.4 ALD GROWTH MECHANISM OF ALUMINIUM OXIDE FROM TMA/ O_3

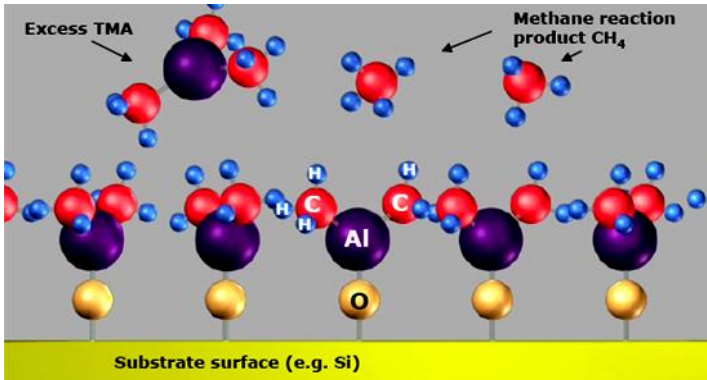
Al_2O_3 depositions were performed on crystalline silicon (c-Si) as a substrate. In subfigure 3.4.1 a, -OH terminated dangling bonds on the surface are shown that allows TMA molecules to form a chemical bond on pulsing of TMA. It was also found that TMA fragments only stick permanently to the surface after protons from the surface migrate to TMA and eliminate one or more ligands as CH_4 . The resulting formation of an Al-O bond is the first step in film growth [Elliott u. a. 2006]. In figure 3.4.1 b, the byproduct was methane molecule also was confirmed in [Goldstein u. a. 2008, p.19530], after reacting with -OH group from the surface. Therefore creating the self terminating reaction until the whole substrate surface was left with no -OH groups; this is the case in ideal conditions and with optimised process parameters. Moreover, excessive TMA molecules were left non-reacted on the surface or on the walls of the chamber. Later that can be removed easily by Ar purge along with methane by products. In figure 3.4.1

Figure 3.4.1 Schematic illustration of an ALD cycle

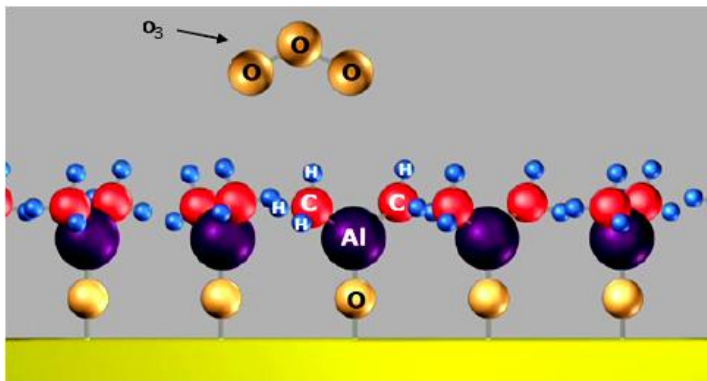
a pulsing of TMA precursor



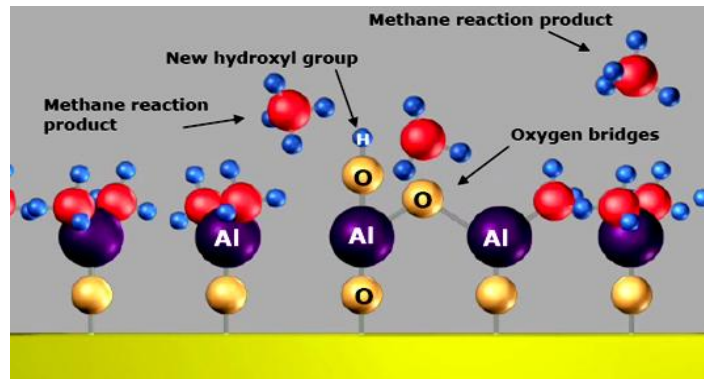
b adsorbed TMA molecules on $-\text{OH}$ terminated substrate sample



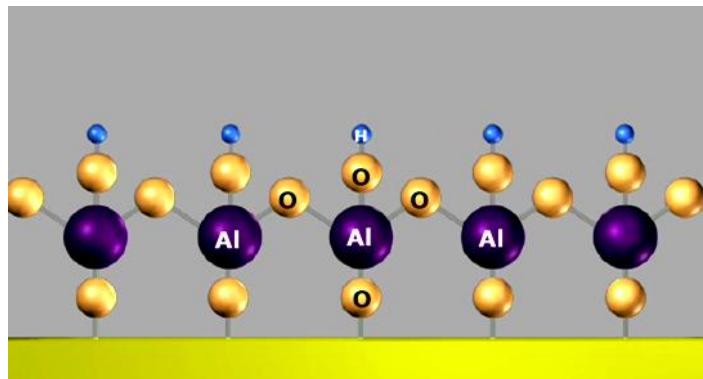
c pulsing of Ozone as a co-reactant



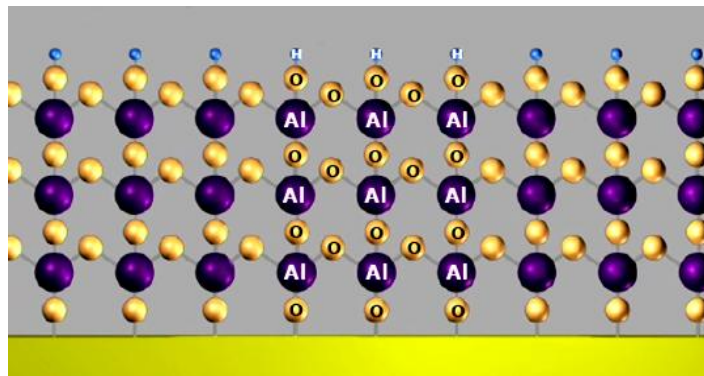
- d after reaction of Ozone molecule with CH_3 ligands of surface absorbed TMA molecule



- e Al_2O_3 monolayer (ML) formation after one complete ALD cycle



- f Al_2O_3 deposited after several ALD cycles



[adapted from cambridge nanotech July]

c, the second reactant ozone was pulsed that acts as oxygen source. Thus after reaction with the monolayer of TMA adsorbate, a layer that looks like in figure 3.4.1 d was obtained. This mechanism was proposed by [Goldstein u. a. 2008, p.19537] along with other reaction by products like carbonate, formate complexes. After the accomplishment of step shown in figure 3.4.1 d, second Ar gas purging was ensured to remove all by products and to obtain a nice Al_2O_3 monolayer shown in figure 3.4.1 e. By performing these pulses over and again, a fine Al_2O_3 thin film of desired thickness that looks similar to figure 3.4.1 f can be obtained.

3.5 GROWTH KINETICS

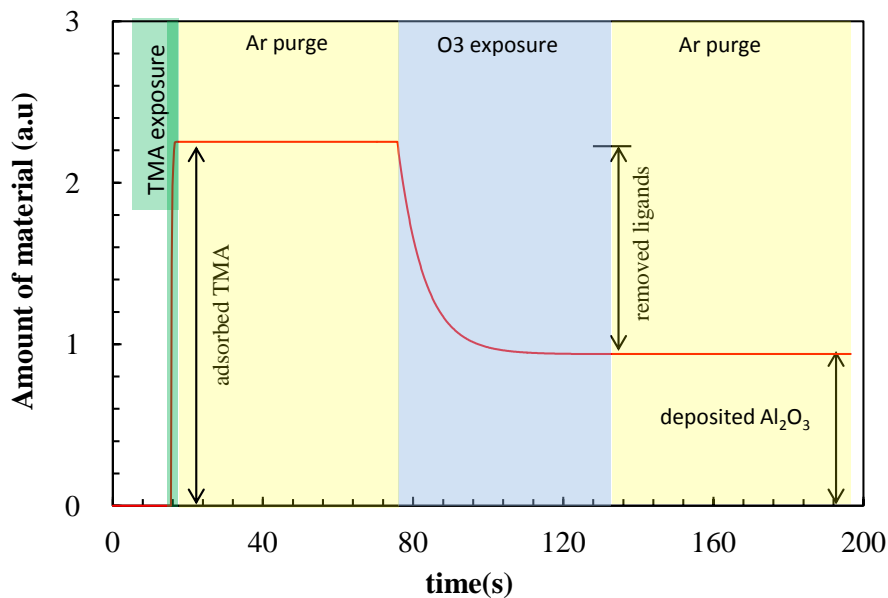


Figure 3.5.1 complete ALD cycle averaged over 10 ALD cycles

The complete ALD process includes many ALD cycles required to deposit the desired amount of Aluminum oxide. Every ALD cycle comprises of four steps as described in section 3.2. Figure 3.5.1 shows the amount of material evolving during one ALD cycle. In this figure every ALD step has been shown with different colors.

Starting with TMA exposure, marked as light green, TMA molecules get adsorbed on the substrate surface until there are no more adsorption sites available. This amount of adsorbed TMA molecules has been marked with an arrow showing ' M_{ads} ', indicating the maximum molecules that can absorb on substrate at particular instance and with unique process parameter conditions. This is the reason for self-limitation in ALD.

Now after this TMA exposure, it is necessary to purge excessive molecules out of the

chamber. This step has been shown in figure 3.5.1 with light yellow mark and is called as Ar purging after TMA exposure. As Argon gas was used to purge the chamber because it is inert in nature. It should also be stated here, that the amount of adsorbed TMA was not dropped in the figure because ideally Ar (due to its inert nature) purge cannot break the chemical bond formed during first step.

The ozone exposure has been shown as light blue in the figure 3.5.1. Ozone starts to react with TMA adsorbate and form various complex intermediates on the surface [Goldstein u. a. 2008, p.19537]. This ligand removal from TMA adsorbate on ozone exposure is denoted by ' L_{rem} '. This curve is assumed to show an exponential decay, which can be approximately defined by a fitting function described in formula 3.3 and will be discussed later in section 7.3.3. Mathematically the growth kinetics described by ' K_{O_3} ' for TMA-Ozone reaction, is the decay rate of the exponential function shown in formula 3.3. The physical meaning of ' K_{O_3} ' is a ligand removal from TMA adsorbate on ozone exposure which have been shown before in figure 3.2.1 d. On completion of this step, all methyl ligands have been removed from the TMA adsorbed surface.

After accomplishment of this step it is now important to remove all the reaction byproducts out of the chamber. Thus the final step of Ar purging after ozone exposure has been followed to clear the chamber. Ar purge causes no damage to the recently formed Al_2O_3 on surface because Ar gas is inert in nature and Al-O bond is sufficiently strong to be damaged by Ar purge.

After completion of one ALD cycle, the amount of Al_2O_3 deposited is denoted as growth per cycle (GPC) that can be described as in formula 3.1, where $T_{thickness}$ and N_{cycles} are total thickness of material deposited and total number of ALD cycles respectively. Cycle time of a complete ALD cycle is described mathematically in equation 3.2, where t_{TMA} , t_{Ar1} , t_{O_3} , t_{Ar2} and t_{cycle} are TMA exposure, Ar pulse time after TMA exposure time, ozone exposure time, Ar pulse time after O_3 exposure and complete ALD cycle time, respectively. Similarly, the two constants ' K_{TMA} ' and ' K_{O_3} ' describe the growth kinetics for TMA adsorption and ligand removal. Theoretically, adsorption of TMA molecules can also be described in terms of exponential growth with K_{TMA} as one of its parameters but due to practical reasons and fast adsorption it was complicated to do the fitting procedure. Therefore, in this project the focus was more on studying the growth kinetics for ozone.

$$GPC = M_{ads} - L_{rem} = T_{thickness}/N_{cycles} \quad (3.1)$$

$$t_{cycle} = t_{TMA} + t_{Ar1} + t_{O_3} + t_{Ar2} \quad (3.2)$$

$$L_{rem} \approx y_0 + A.exp(-K_{O_3}t) \quad (3.3)$$

3.6 COMPARISON OF TMA/O₃ AND TMA/H₂O – A LITERATURE SURVEY

A brief literature review is devoted to this section, that covers only small part of the entire work done on Al₂O₃ from TMA and H₂O/O₃. According to previous research done one cannot really tell which co-reactant (O₃/H₂O) is better because it depends on the chamber design, quality of both the precursors etc. But one can obtain the same results with both the precursors by tweaking other parameters like temperature, pressure etc.

Various growth mechanisms for TMA/H₂O and TMA/O₃ have been proposed by many researchers. In [Delabie u. a. 2012] the growth mechanism for TMA/H₂O was proposed. where [Elliott u. a. 2006] [Goldstein u. a. 2008] proposes the mechanism for TMA/O₃. In case of TMA and H₂O the growth is inhibited from the second reaction cycle and then increases back to the steady value (4 Al atoms/nm²) after approximately 20 reaction cycles [Delabie u. a. 2012, p.3]. It has been also shown in [Soto 1991, p.2695] that there are two phases of growth procedures for TMA/H₂O so called interface and bulk formation. On the other hand, for TMA/O₃ there is no island formation but layer by layer growth mechanism. It also does not show any inhibited first reaction cycles [Park u. a. 2003].

ALD experiments shown in [J. Spiegelman u. J. Sundqvist 2011, p.25] assure the replacement of ozone with water vapor is very efficient, self-limiting and increased the film growth rates by 14.5%. Saturation pulse times were similar between the two oxidants as this is directly related to gas flow dynamics in the specific ALD process chamber. However the company RASIRC equipment was used in this case to generate ultra pure water vapors [J. Spiegelman u. J. Sundqvist 2011, p.25]. High electrochemical potential of ozone results in fast reaction rates at relatively low temperatures as compare to water which is less reactive [Hans sundstrom 2005, p.2]. Also a little enhancement in growth rate has been seen after treating the growing surface with excessive water (H₂O) (meaning long water pulse time or increased water flow) throughout TMA/H₂O process [Elliott u. a. 2006]. However, the use of ozone as a second reactant does not significantly alter the growth rate when compared to water based Al₂O₃ ALD films [Kim u. a. 2006].

It was also found that substrate temperature plays crucial role rather than a choice of oxygen source while describing Al₂O₃ film properties like film thickness uniformity, step coverage and growth rate. In case of O₃-based Al₂O₃ films, step coverage was found to increase with increasing substrate temperature unlike H₂O-based Al₂O₃ films, where the growth rate drops beyond 350°C. Moreover in case of TMA/O₃, the step coverage was determined nearly 100% for the films deposited at a higher substrate temperature

450°C [Kim u. a. 2006]. On the contrary, for both oxygen precursors, the molar growth rate per cycle decreases with increasing temperature, and at no temperature does the O₃ process yield faster growth than the H₂O process [Elliott u. a. 2006].

It is also important to do a comparison of both oxygen sources in terms of quality and defects in grown Al₂O₃ films. Al₂O₃ films grown from TMA and ozone had lower carbon and hydrogen impurities as compared to TMA and water [Goldstein u. a. 2008; Jakschik u. a. 2003; Kim u. a. 2006] because of absence of hydrogen in ozone molecule [Hans sundstrom 2005]. It has been demonstrated that the Al₂O₃ films prepared with O₃ have significantly less amount of defect states like Al–Al and –OH bonds compared to those prepared with water [Goldstein u. a. 2008; Jakschik u. a. 2003; Kim u. a. 2006] [Kim u. a. 2002, p.6742]. At low temperature, the interaction of H₂O with Si seems to produce a thicker oxygen–rich interfacial layer, which adheres poorly to the Si substrate [Jakschik u. a. 2003]. In contrary to, O₃ as the oxygen source yields uniform films than H₂O based Al₂O₃ films [Jakschik u. a. 2003] but lower–quality films than those grown from TMA/H₂O; the films are less dense and rougher, especially at low growth temperatures. However, use of O₃ as oxygen source yields thicker films at low temperature, because of their lower density, correlated with the existence of voids in the alumina layers [Elliott u. a. 2006, p. 3764 – 3767]. By contrast, treatment of the growing surface with excess H₂O in the TMA/H₂O process ensures homogeneous surface –OH groups, a denser and smoother film, regardless of temperature.

Also the Al₂O₃ films prepared with O₃ shows 1–2 order lower leakage current density compared with the Al₂O₃ film prepared with H₂O. The wet etch (due to H₂O as co-reactant) rate has been found to have little effect on Al₂O₃ films prepared using O₃ thus they are more stable to environment conditions as compared to those prepared with water [Kim u. a. 2002] [Ritala 2002 p.120].

Last but not least, lower TMA consumption were observed when using ozone than when using water [Elliott u. a. 2006]. Another reason to prefer ozone as reactant than water is that water molecules stick to the walls of the inside chamber and is hard to purge [Elliott u. a. 2006, p.3764].

4 SPECTROSCOPIC ELLIPSOMETRY

4.1 INTRODUCTION

Ellipsometry was first developed and defined mathematically by Drude in 1887. Later this technology has been exploited very much since mid 19th century and still research is going on to make it better [Fujiwara 2007, p.8]. Spectroscopic Ellipsometry is an optical technique used for analysis and metrology of the various samples like dielectrics, semiconductors, metals, superconductors, etc. The measured response depends on optical properties and thickness of individual materials. Thus, ellipsometry is primarily used to determine film thickness and optical constants. It is also applied to characterize composition, crystallinity, roughness, doping concentration, and other material properties associated with a change in optical response. The name 'ellipsometry' comes from the fact that polarized light upon reflection with sample becomes 'elliptical' and spectroscopic comes from the measurements that are carried out in the wide range of electro magnetic (e.m.) spectrum (200nm to 1700nm approx.) [Fujiwara 2007, p.1]. It has both capabilities for in-situ as well as ex-situ measurements. In situ is Latin for "in the place" while ex-situ means "off-site". In situ measurements of the surface can monitor the layer-by-layer growth that occurs exactly in ALD process. In situ SE monitoring has been applied to many deposition techniques (e.g., MBE, MOCVD, sputtering, ALD etc.) [Dale E. Morton u. a. 2002, p.2].

4.2 MEASURING PRINCIPLE

In Ellipsometry, a beam of linearly polarized light with known wavelength is incident onto a sample of interest as shown in figure 4.2.1. Upon reflection from surface of sample, the polarization state of light is changed to an elliptically polarized light. This change in polarization state of light is measured by two parameters (Ψ , Δ as shown in figure 4.2.1) and are known as ellipsometry parameters or angles. This is the basic principle of Ellipsometry and is described briefly as below.

The polarization state of light can be described by the coordinates of p-(parallel) and s-(senkrecht from German) polarizations. For convenience, the ratio ρ of the Fresnel amplitude reflection coefficients for p- and s- polarized light can be defined as $\rho = r_p/r_s$. Where r_p , r_s are the Fresnel reflection coefficients for the p- and s- polarized light wave, respectively. Both r_p , r_s are complex, so is the ratio ρ , which is expressed in terms of two ellipsometry parameters (Ψ , Δ) as follows [Fujiwara 2007, p.81 - 84].

$$\rho \equiv \tan(\psi) \cdot e^{i\Delta} \quad (4.1)$$

The raw measurement is determined by two values, amplitude ratio called Psi (Ψ) and

phase difference is denoted by Delta (Δ). Figure 4.2.1 illustrates the measurement principle of ellipsometry. Where linearly polarized incident light beam E falls on the sample at angle θ to the plane of incidence as shown in figure 4.2.1 and contains both parallel (E_{ip}) and perpendicular (E_{is}) polarized wave components. Where $E_{is} = E_{ip}$ for linearly polarized light, since the amplitudes of p- and s- polarizations are the same and the phase difference between the polarizations is zero. This incident light beam is reflected from the sample surface and becomes elliptically polarized with E_{rs} and E_{rp} reflected s- and p-polarized light beam components respectively. And it undergoes a significant change in its amplitude and phase for both p- and s- polarized states [Fujiwara 2007, p.82]. The change in polarization is known as the ellipsometry measurement, commonly written as:

$$\rho \equiv (E_{rp}/E_{ip})(E_{rs}/E_{is}) \quad (4.2)$$

For accurate Ellipsometry measurements, a linear polarized light wave is irradiated onto a sample at the Brewster angle (as the difference between r_p and r_s is maximized at Brewster angle θ_B , hence the measurement sensitivity is maximum too).

This is the basic principle of ellipsometry measurement. Then measured (Ψ, Δ) values are used to calculate other optical parameters [Dale E. Morton u. a. 2002, p.3] [Fujiwara 2007, p.40]. Particularly, when a sample structure is simple, the amplitude ratio Ψ is characterized by the refractive index (n), while Δ represents light absorption described by the extinction coefficient κ . In this case, the two values (n, κ) can be determined directly from the two ellipsometry parameters Ψ and Δ obtained from a measurement [Fujiwara 2007, p.84].

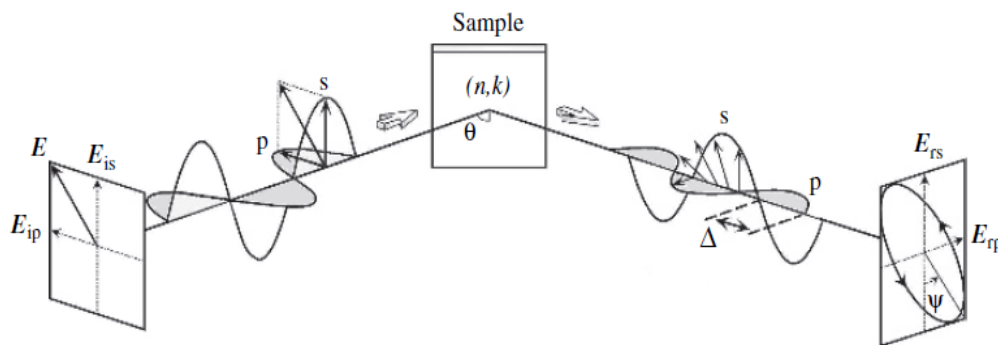


Figure 4.2.1 Schematic illustration of experimental setups of spectroscopic ellipsometry. Linearly polarized light is incident to a sample substrate with incident angle of θ . The ellipsometry parameters Ψ and Δ , which represent the ratio of amplitudes of s- and p-polarized components of the incident light and the phase difference between them, respectively [Fujiwara 2007, p.82]

4.3 FITTING AND MODELS

SE software Models

SE is a model based analysis technique. In general models are classified into two types; optical layer stack (OLS) model and material model. OLS models consist of layers of different materials e.g. single layer, multi layer etc. with different film parameters e.g. as shown in figure 4.3.1 and these layers can be further elaborated with roughness and graded indices. OLS model represents the basic structure of the deposited material on sample substrate [J.A. Woollam Co. 2011, p.3-42]. A specific OLS model depends on best assumption made according to a specific deposition process. For instance, in this research Al_2O_3 was deposited on silicon substrate (with natOx on it more detail in figure 7.4.3).

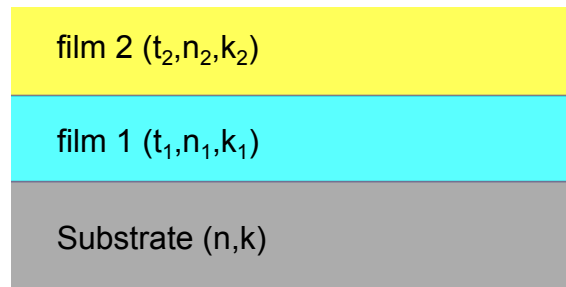


Figure 4.3.1 Schematic representation of a simple optical layered model with two films, parameterized by thickness (t_1, t_2) and optical constants (n, k) [adapted from J.A. Woollam Co. 2011, p.3-43]

The material model is a model that represents the type of material and its properties e.g. dielectric, semiconductor etc. According to the optical properties of sample an appropriate dielectric function model is selected. The various dielectric function models are Lorentz, Sellmeier, Cauchy, Tauc-Lorentz, and Drude models. Basically, all these models are derived from the Lorentz oscillator model [Fujiwara 2007, p.160].

Fitting procedure

Figure 4.3.2, shows the detailed characterization of physical properties by spectroscopic ellipsometry. It describes Psi and Delta, are the only two values determined directly by SE. In SE, the obtained raw data (Ψ, Δ) is meaningless without performing any modelling. The interesting characteristics such as film thickness, surface roughness and optical material parameters can be determined only by optically modelling the near-surface

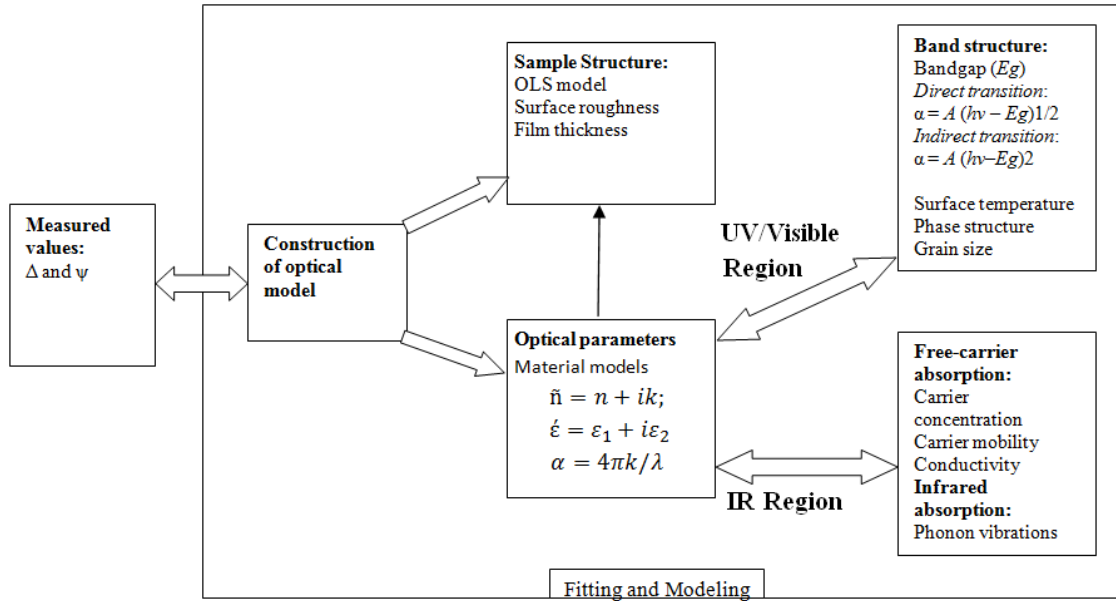


Figure 4.3.2 characterization of physical properties by spectroscopic ellipsometry [adapted from Fujiwara 2007, p.4]

region of the sample [Jellison 1998, p.1]. In general, three steps are involved while fitting SE data, to obtain valuable information on various thin film parameters. These steps are as follows:

1. Choosing an optical layer stack (OLS) model (OLS model specific to this research project is shown in figure 7.4.3). After obtaining a specific OLS model, it is required to define the material model for each layer that provides the information on various optical parameters and absorption coefficient (α) [Fujiwara 2007, p.161]. Various material models can be selected from the inbuilt library of CompleteEASE software.
2. After defining the model, fitting of the optical layer parameters like thickness and temperature (also shown in figure 7.4.3) is an important step. The CompleteEASE software runs some algorithms like Levenberg-Marquardt method [J.A. Woollam Co. 2011, p.3-46] to improve the agreement between the measured and model generated SE data [J.A. Woollam Co. 2011, p.3-42].
3. If the modelled data and generated data fits well upto specific interest. Then the fitting is acceptable and various information is evaluated. If the fit is not acceptable then it is required to find a suitable model or modify the fit parameters.

MSE definition

During optical modelling (SE data evaluation), the main goal is to obtain the minimum mean squared error (MSE). MSE describes how nicely the model-generated data fits the measured Ψ , Δ values. Mathematically, MSE is defined by equation 7.3 [Himcinschi u. a. 2001, p.808].

$$MSE = \sqrt{\frac{1}{2N - M} \sum_{i=1}^N \left[\left(\frac{\Psi_i^{mod} - \Psi_i^{exp}}{\sigma_{\Psi,i}^{exp}} \right)^2 + \left(\frac{\Delta_i^{mod} - \Delta_i^{exp}}{\sigma_{\Delta,i}^{exp}} \right)^2 \right]} \quad (4.3)$$

Where 'N' is number of experimental (Ψ , Δ) pairs, 'M' is number of fit parameters and σ is the standard deviation on the experimental data points [Himcinschi u. a. 2001, p.808]. The lower the MSE, the better is the fit agreement between generated and modeled data. So for a best fit, the MSE value is the lowest value possible [J.A. Woollam Co. 2011, p.3-45]. For accurate determination of model parameters, MSE should be constant over the desired range of wavelength and should be minimum among various allowed OLS models for a particular deposition [J.A. Woollam Co. 2011, p.3-44] [Dale E. Morton u. a. 2002, p.1].

4.4 ADVANTAGES AND LIMITATIONS

Ellipsometer provides numerous advantages over conventional techniques based on reflection and absorption. First it is ratio based technique that can be measured accurately even in less intense light conditions. Thus it is capable to measure precisely even if there are some intensity fluctuations in the source [Dale E. Morton u. a. 2002, p.1]. Secondly, it is highly precise in measuring thickness with the sensitivity close to 0.1 Å. It is fast in measurement and the delay can also be introduced (in case of triggered measurements). Thus it is flexible in nature. Third advantage is its in-situ capabilities and determining the real time measurements [Fujiwara 2007, p.3].

Ellipsometry is used to measure a wide variety of thin films. There is no restriction on the type of material measured: dielectrics, semiconductors, metals, organics, and composites of materials etc. provided that light reflects from the surface [Dale E. Morton u. a. 2002]. It can measure an isotropic, anisotropic, homogenous and graded film coatings. Spectroscopic ellipsometry can even be applied to multilayer structures, with films of different materials. Moreover, substrate temperature, quality, absorption and desorption of material can also be measured [B. Johs u. a. 1999]

However, SE has few limitations including necessity of a correct optical model for an-

alyzing the data, hence data analysis is little bit complicated. In combination with array scan technique, it is possible to analyze the whole wafer surface area of 300mm or more but at the expense of time. With help of SE, it is difficult to characterize the optical constants for material with low absorption coefficients[Siah u. a. 2013, p.452]. If the coatings are too rough, it scatters the probe beam away from the detector, which prevents spectroscopic ellipsometry measurements[Dale E. Morton u. a. 2002]

The upper thickness limit for SE measurement depends on the wavelength used and type of material. For thick transparent films, many data oscillations become difficult to perceive at shorter wavelengths but are more resolvable in longer wavelength range. Thus, by using near infrared or even mid-infrared measurements one can measure films up to 50 microns thick. However, this range is beyond a typical SE measurement. The preferred limit for most visible-to-near infrared measurements is less than 5 microns. Even for films that are 1 to 5 micron thick, it is best to measure with multiple angles of incidence to have a unique thickness solution[B. Johs u. a. 1999]. For metal and absorbing films, the upper detection limit is below 100 nm which is dependent on extinction coefficient(κ).

5 X-RAY PHOTOELECTRON SPECTROSCOPY

5.1 INTRODUCTION

XPS is a kind of electron spectroscopy in which a sample is irradiated with a beam of mostly monochromatic x-rays and then measuring the energies of resulting photoelectrons. In 1887, the photoelectric effect was discovered by Heinrich Rudolf Hertz and in year 1905 explained by Albert Einstein. In year 1954, a Swedish physicist Kai Siegbahn recorded the first high-energy-resolution XPS spectrum of cleaved sodium chloride (NaCl). A few years later in 1981, Siegbahn won Nobel Prize for developing the method of electron spectroscopy for chemical analysis (ESCA), now known as XPS [Skoog 1985, p.538].

5.2 XPS MECHANISM

Surface analysis by XPS is accomplished by irradiating mono-energetic x-rays and analyzing the electrons emitted from the surface. Normally, MgK α and AlK α x-ray sources are used with 1253.6 eV and 1486.6 eV energies, respectively. These x-rays penetrate the sample surface and interact with atoms on the surface by photoelectric effect. The emitted photoelectrons have kinetic energy given by equation (5.1)

$$E_k = h\nu - E_b - \phi \quad (5.1)$$

Where, $h\nu$ is energy of exciting photons and E_b is binding energy of atomic orbital from which electron originates and ϕ is known as work function [Wagner u. Muilenberg 1979, p.4]. In the XPS detector the (E_k) kinetic energy and number of electrons that escape from the top (1 to 10 nm) layer of material is measured. A schematic shown in figure 5.2.1 depicts the photoelectric effect.

5.3 XPS ANALYSIS

XPS spectrum is a plot of the number of electrons detected (ordinate) versus the binding energy of those detected electrons (abscissa). Each element produces a characteristic set of XPS peaks at characteristic binding energy values that corresponds to each element that exists in or on the surface of the material that is being analyzed. These characteristic peaks correspond to the electron configuration of the electrons within the atoms, e.g., 1s, 2s, 2p, 3s, etc. The number of detected electrons in each of the characteristic peaks is directly related to the amount of element within the irradiated area (vol-

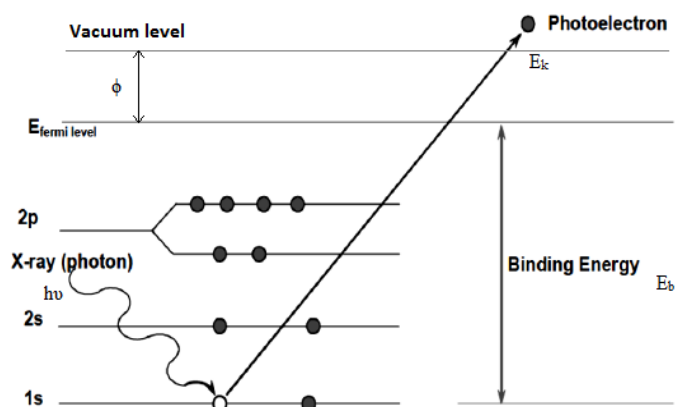


Figure 5.2.1 Diagram of photoelectric effect in XPS

ume). To generate atomic percentage values, each raw XPS signal must be corrected by dividing its signal intensity (number of electrons detected) by a "relative sensitivity factor" (RSF) and normalized over all of the elements detected.

To count the number of electrons at each kinetic energy value, with the minimum error, XPS must be performed under ultra-high vacuum (UHV) conditions because electron counting detectors in XPS instruments are typically one meter away from the material irradiated with X-rays. It is important to note that XPS detects only those electrons that have actually escaped within the vacuum of the instrument. The photo-emitted electrons that have escaped into the vacuum of an instrument are those that originated from within the top 10 to 12 nm of the material layer. For most applications, in-vacuo XPS analysis is efficient and a non-destructive technique (no sputtering is required in case of in-vacuo sample transfer right after finishing the process) that measures the surface chemistry of any material.

5.4 ADVANTAGES AND LIMITATIONS

It is quantitative and surface chemical analysis technique that measures the elemental composition, empirical formula, chemical state and electronic state of the elements that exist within a material. It is non destructive surface analysis technique where the sample surface is not altered. The biggest advantage is its surface and element sensitivity (parts per 1000)[Andrade 1985]. It is easy to understand while the instrument works with a direct interpretation of its theory. XPS is widely used to analyze inorganic as well organic compounds, semiconductors, polymers, ceramics, bio-materials and many others. XPS is very reliable technique that provides with high information content for samples under test[Andrade 1985, p.106].

However, there are few limitations. For effective analysis, samples are analyzed in Ultra high vacuum (UHV, $P \leq 10^{-7}$ Pa). The experimental setup itself is very costly and must be handled with care. The instrument is complex in design. The biggest disadvantage is that we cannot detect hydrogen and helium atoms [Andrade 1985, p.106]. For thorough analysis of some samples it can be very slow. Sometimes the charge on the sample surface can be a problem that may shift the peaks in either directions. This can generate some confusion while analyzing some elements.

6 ATOMIC FORCE MICROSCOPY

AFM is a very high-resolution type of scanning probe microscopy, with demonstrated high resolution on the order of fractions of a nanometer. AFM consists of a cantilever with a sharp tip at its end that is used to scan the test sample surface. The cantilever is typically silicon or silicon nitride with a tip radius of curvature on the order of few Angstroms. When the tip is brought into proximity of a sample surface, forces between the tip and the sample lead to a deflection of the cantilever according to Hooke's law. Depending on the situation, forces that are measured in AFM include van der Waals forces, electrostatic forces, magnetic forces, Casimir forces etc. Typically, the deflection is measured using a laser spot reflected from the top surface of the cantilever into an array of photodiodes. Other methods that are used include optical interferometry, capacitive sensing or piezoresistive AFM cantilevers [Binnig u. Quate 1986].

AFM gives topographical scan of a sample surface. The micro and nano-scale features of the sample can be observed, portraying the roughness of the material. If the tip was scanned at a constant height, a risk would exist that the tip collides with the surface, causing damage. Hence, in most cases a feedback mechanism is employed to adjust the tip-to-sample distance to maintain a constant force between the tip and the sample. Traditionally, the sample is mounted on a piezoelectric sensor that can move the sample in the z direction for maintaining a constant force, and the x and y directions for scanning the sample.

The AFM can be operated in a number of modes, depending on the application. In general, possible imaging modes are divided into static (also called contact) modes and a variety of dynamic (non-contact or "tapping") modes where the cantilever is vibrated throughout the measurement. In non-contact mode, the tip of the cantilever does not contact the sample surface [Zhong u. a. 1993, p.L688]. The cantilever is instead oscillated at either its resonant frequency (frequency modulation) or just above (amplitude modulation) where the amplitude of oscillation is typically a few nanometers (<10 nm) down to a few picometers [Gross u. a. 2009]. The van der Waals forces, which are strongest from 1 nm to 10 nm above the surface, or any other long range force which extends above the surface acts to decrease the resonance frequency of the cantilever. This decrease in resonant frequency combined with the feedback loop system maintains a constant oscillation amplitude or frequency by adjusting the average tip-to-sample distance. Measuring the tip-to-sample distance at each (x,y) data point allows the scanning software to construct a topographic image of the sample surface [Binnig u. Quate 1986].

II EXPERIMENTAL PART

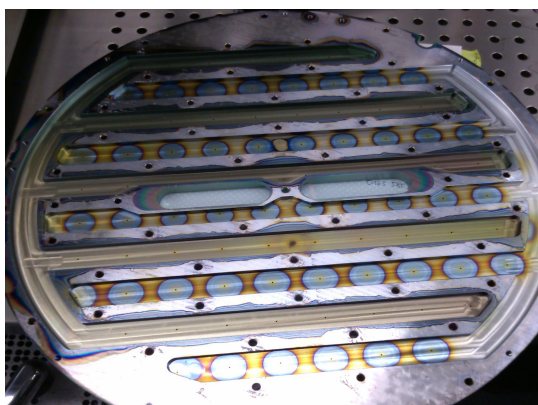
7 METHODOLOGIES

7.1 EXPERIMENTAL SETUP

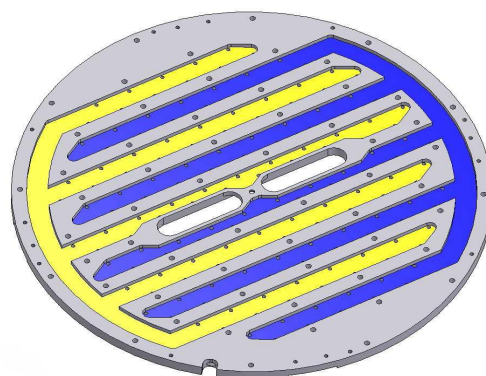
All experiments in this student project were performed on a top injection ALD-300 reactor type from the company FHR Anlagenbau GmbH and are described in detail in chapter 8. Figure 7.1.2 shows the ALD-300 tool, that consists of two process chambers, a load lock and a wafer transport system [more details in Schmidt u. a. 2008, p.528]. All chambers are separated from each other with the help of vacuum locks that are controlled pneumatically. The ALD chamber is a warm wall reactor with shower head for exposure of gases. Shower head type of exposure is used because it provides with a uniform flux flow-inside the reaction chamber [Kim u. a. 2003, p.734].

Two kinds of shower head designs were used to study the influence of flow dynamics on pulsing and purging times. Better flow dynamics may lead to faster growth with better conformality, homogeneity, quality and less contaminations [Kim u. a. 2003, p.734]. In general (see figure 7.1.1), both shower head designs implemented two different gas channels to keep the reactants (TMA and ozone) separate and are entwined in a comb like structure. A slight continuous Argon gas flow is used to prevent any kind of deposition occurring inside these channels.

Type I shower head design has less number of pin holes per each gas channel. In figure 7.1.1 a, it can be seen very clearly that all the holes lie in the middle of channels. While on other hand in figure 7.1.1 b, Type II shower head design has holes almost twice in number as compared to Type I. Also the holes are not in the middle of channels but on the side walls, forming like a zigzag pattern. The results for Al_2O_3 ALD depositions for both shower head designs will be discussed in chapter 8.



a back side of Type I shower head design



b back side of Type II shower head design

Figure 7.1.1 Comparison of Type I (a) and Type II (b) shower head designs

Various measurement equipments are attached to both ALD chambers. This includes spectroscopic ellipsometer (SE), X-ray photoelectron spectroscope (XPS), UV photoelectron spectroscope (UPS) and an atomic force microscope (AFM). The SE (shown in figure 7.1.2 with colored rectangular blocks; red being the light source and blue as detector part) is attached to the ALD metal chamber for in-situ access. Direct surface analysis is done with the help of XPS and AFM after sample transfer within a high vacuum ($\approx 10^{-5}$ Pa).

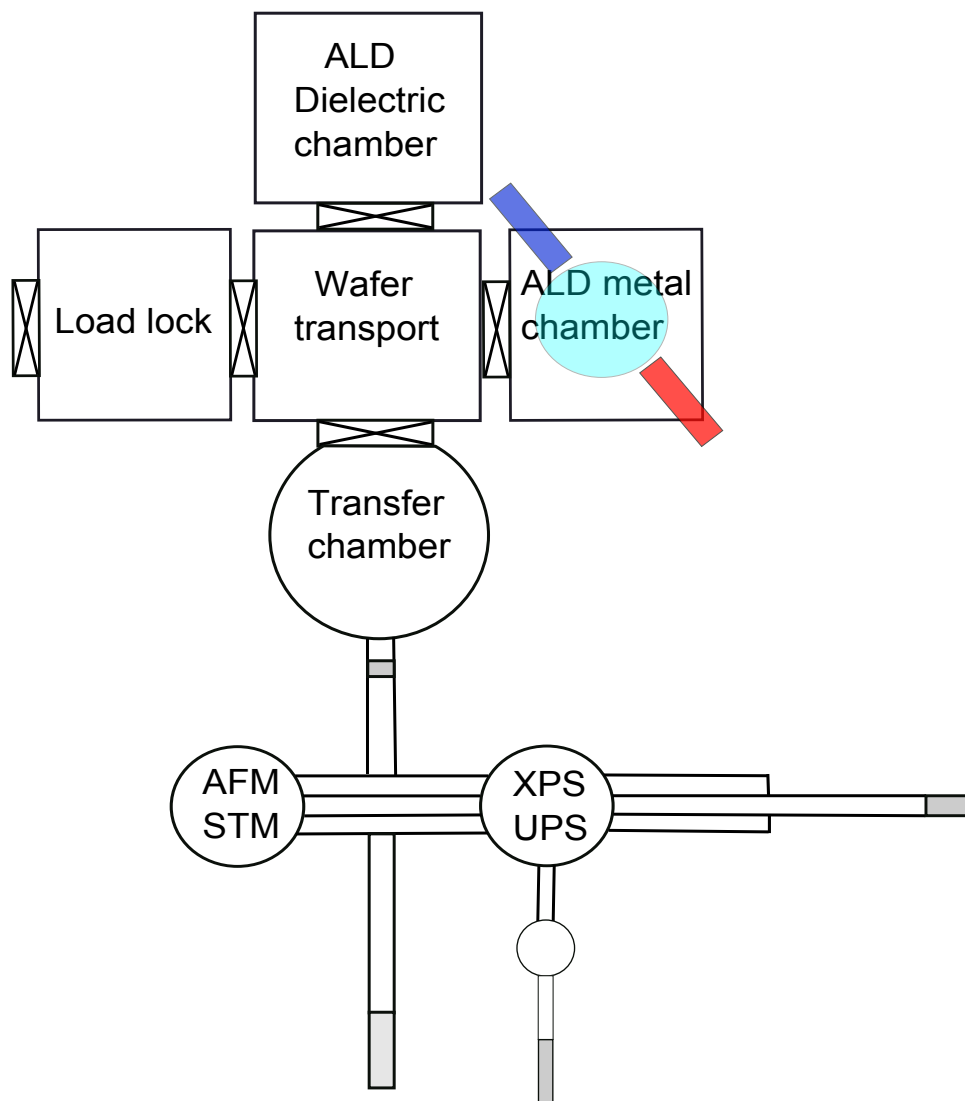


Figure 7.1.2 Schematic diagram of ALD-300 chamber from FHR Analgenbau GmbH with surface characterization and analysis system from Omicron Nanotechnology GmbH

7.2 ALD PROCESS

During all experiments, a substrate of crystalline silicon (c-Si) with native oxide (natOx) was used. The size of substrate samples were approximately $1\text{ cm} \times 1\text{ cm}$. The substrate samples were cut into small coupons from original 8 inch wafer. Al_2O_3 depositions were performed by thermally enhanced ALD technique. The surface reactions were accomplished by two reactants; TMA and Ozone. In each experiment 100 ALD cycles were performed. Argon gas was used to purge the chamber and as a carrier gas for TMA precursor. All gases except ozone were controlled by MFCs. However, O_3 flow was fixed to a particular value with the help of manually controlled needle valve because over time O_3 can damage the built-in MFC. TMA-bubbler temperature (ϑ_{TMA}) was kept at $16\text{ }^\circ\text{C}$ according to the specifications provided by the vendor. Substrate heating was controlled with the help of resistive heater attached at the bottom of substrate holder. To obtain the desired substrate temperature ($\vartheta_{\text{Substrate}}$) pre-heating was always done at higher pressure that is 300 Pa for 15 mins to fasten the heating process and then stabilizing the temperature by reducing the pressure to process conditions (e.g. 200 Pa , $150\text{ }^\circ\text{C}$)[more details in appendix and Junige u. a., p.2].

7.3 EXPERIMENT DESIGN

In order to investigate and study the interdependency of ALD process parameters, the following process parameters were varied: TMA exposure time, Argon purge time after TMA exposure, ozone exposure time, Argon purge time after ozone exposure, respectively. These exposure and purging variations were helpful to study the optimum cycle time for one complete ALD cycle. This optimum cycle time is necessary to ensure the saturated monolayer formation of TMA adsorbate, minimum time required to purge the excessive TMA molecules and reaction by-products from chamber, minimum ozone exposure time required to have a complete reaction with TMA adsorbate on the surface and minimum time required to purge the reaction by-products. Varying the exposure and purge times of both reactants provide the kinetic ALD characteristic curves (discussed in 8.2.1 - 8.2.4 subsections), i.e. the saturation of both ALD half-reactions and the purging behaviour, respectively. It also gives the minimum amount of precursor needed. The GPC tends to saturate at a point where no chemisorption is possible anymore. In an ideal case, further extension of exposure or purging times (keeping all other process parameters constant) will not improve the GPC or quality of thin films [Nalwa 2002, p.140].

Other process parameters that were varied are total process pressure, O_3 gas flow and deposition temperature. Studying the temperature characteristics plays a crucial role in

the development of an ALD process, as it reveals the temperature window in order to achieve a saturated and thus stable GPC. Finally, the effect of varying above mentioned process parameters and their interdependencies were studied by taking various ALD characteristic curve attributes into account. The ALD characteristic curve attributes are GPC, growth kinetics for ozone reaction step, ligand removal and TMA adsorption. For instance, the effect of varying substrate temperature was noticed by recording the GPC, TMA adsorption and growth kinetics for ozone step (see figure 8.3.6). For studying the impact of various process parameters on an ALD process, only one parameter was varied at a time by keeping others constant (see Appendix) [as described in Nalwa 2002, p.139]. All other process parameters were kept constant in order to achieve similar process conditions inside the reaction chamber.

As one of the most important ALD characteristic curve attribute, the growth per cycle (GPC) has been defined as the film thickness increment resulting from the application of one single ALD cycle (i.e. the exposure and purging of precursor and co reactants, respectively) [Puurunen 2005]. However in recent research, commonly a cumulative GPC has been determined by total film thickness over the total number of ALD cycles applied for the deposition of thicker measurable film. Nevertheless in this report, a real GPC measurement was incorporated by studying a film thickness increment after completion of each ALD cycle. This is one big advantage of *in situ* SE measurements reported in this research project.

Temperature was varied from 100°C to 500°C in steps of 100°C. This temperature was a set point temperature but the actual surface temperature ($\vartheta_{\text{Surface}}$) was obtained by fitting *in-situ* SE data as shown in table A.1 (in section A of Appendix). The chamber pressure was varied from 100Pa to 500Pa in accordance with table B.1. The ozone flow was varied from 50sccm to 500sccm [as described in table A.2]. Ozone flow was controlled with the help of a needle valve by observing the chamber pressure. The effect on chamber pressure was noticed by changing the oxygen flow (in sccm) with the help of a needle valve position. Ozone flow was assumed to show the same effect on chamber pressure. Thus Ozone flow was indirectly controlled and set to its corresponding value [as shown in table A.2] for a particular set of process parameters to accomplish one ALD process.

However, in most ALD processes a compromise between growing a desirable amount of material with acceptable quality and given time as well as temperature regime has to be found. As the ALD characteristic curves themselves do not include any information about the film quality. A further characterisation (for example by XPS, AFM, etc.) of film properties is needed.

7.4 SPECTROSCOPIC ELLIPSOMETRY

7.4.1 Tool and software

A Rotating Compensator Ellipsometer (*RCE*) of type M-2000 FI from the company J. A. Woollam Co. Inc, was mounted right on the ALD metal chamber. *RCE* is one of the possible configurations in SE with many advantages over other configurations like Rotating Analyser Ellipsometer (*RAE*). *RCE* has uniform sensitivity over an entire $\Psi(0^\circ - 90^\circ)$ and $\Delta(0^\circ - 360^\circ)$ range [Aspnes u. Hauge 1976, p. 949 - 953] and thus, measures these both ellipsometric angles more accurately. Type M-2000 FI ellipsometer covers 673 wavelengths of spectral range from 190nm to 1690nm [J.A. Woollam Co. 2011].

Figure 7.1.2 shows the red block mounted on metal chamber at 64° of angle of incidence (AOI), which is a 75 Watts Xe arc lamp light source (FLS-350) and blue is detector part of SE tool. While measuring in-situ data, the light beam passes through a special pre-strained glass windows with no shutters installed. A continuous Ar gas flow prevents the windows from any undesired depositions.

The CompleteEASE (ver. 4.90) software was used in these experiments to measure and evaluate the in-situ data. The details of the analysis procedure can be found in the literature [J.A. Woollam Co. 2011; Jakschik u. a. 2003; Kim u. a. 2006].

7.4.2 Data acquisition

A CompleteEASE software that runs on a local computer acquires in-situ data from the SE hardware through a TCP/IP link. Before measuring the in-situ data, a system check was performed once. A system check is a most common method for calibrating the ellipsometer [J.A. Woollam Co. 2011, p.12-358]. A system check is a software automated process that calculates a coarse AOI, includes in- and out-of-plane window effects and write back to hardware settings. This procedure automatically corrects the acquired spectra of Ψ and Δ . SE data acquisition can be classified in to two broad categories as described below.

Time-discrete data acquisition

In time-discrete data acquisition mode a special kind of synchronisation device between the ALD tool and CompleteEASE software is required that allows the triggering of data acquisition at the beginning of each purging step.

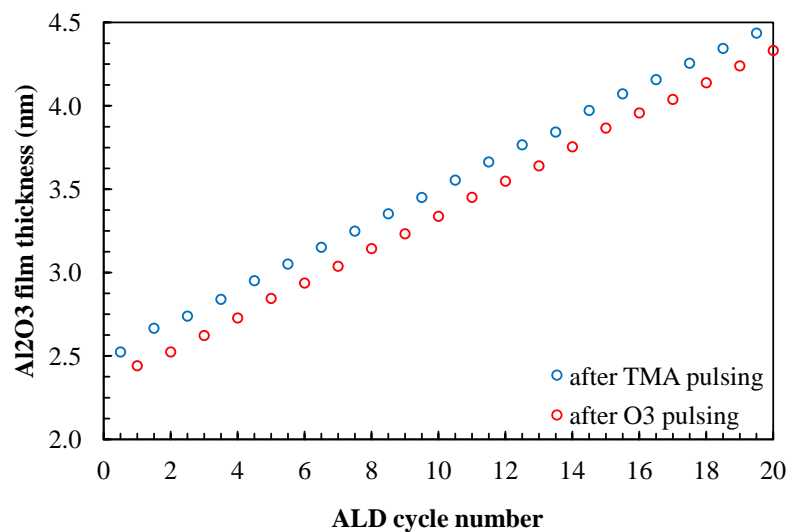


Figure 7.4.1 course of the optical layer thickness as revealed by iSE time-discrete data acquisition over the Al₂O₃ ALD cycle number

In chapter 8, two shower head designs are compared in terms of their purge behaviour, by employing time-discrete SE measurements. Figure 7.4.1 plots the evaluated optical layer thickness in the discretized course of the Al₂O₃ ALD cycle number. Blue and red data points show the measurements that were triggered to the Ar purge right after TMA and Ozone exposures, respectively. Red data points depict the optical layer thickness after completion of the O₃ exposure (second ALD half-reaction). In other words, red data points show the amount of Al₂O₃ deposited upon completion of each ALD cycle. From figure 7.4.1, the GPC can be easily extracted by just subtracting the two consecutive red data points.

Time-continuous data acquisition

Evolution of the film thickness for ALD grown Al₂O₃ over the process time was also monitored with the help of in-situ real-time SE (irtSE) in a time-continuous manner. In time-continuous acquisition, each data point was acquired with a sampling rate of 0.8 s. This sampling rate was enough to measure the whole data set values through out a complete ALD process time. The time-continuous acquisition can also be selected either for fast or high accuracy mode. For high accuracy with standard configuration mode the polarizer moves to two positions and measures raw data accurately by cancelling the alignment issues [J.A. Woollam Co. 2011, p.11-347]. Also it takes twice as much time per measurement but significantly improves the accuracy. SE tool allows to monitor the various film properties like substrate temperature, thickness etc in real time. Figure 7.4.5 a plots the change in optical layer thickness versus the time continuous ALD process time for 10 ALD cycles. After acquiring data the next step is to evaluate it and is described in section 7.4.3.

Comparison of time-discrete and time-continuous data acquisition

Figure 7.4.2 exploits time-discrete and time-continuous data acquisition capabilities of iSE. For time-continuous SE measurement, a decremental of optical layer thickness (inverted blue region in figure 3.5.1) was plotted to compare with GPC saturation curve for O_3 exposure time that was obtained from time-discrete SE measurements i.e. for each data point the thickness slope was calculated after applying 10 ALD cycles. Figure shows that growth kinetics can be revealed for both type of measurements. The both Kinetic ALD characteristic curves overlay on each other showing a saturation around 55 seconds of O_3 exposure time. However, one big advantage of time-continuous SE measurement is that it has more data points (acquiring each data point almost every one second) in shorter time as compare to time-discrete SE measurement and thus providing more information.

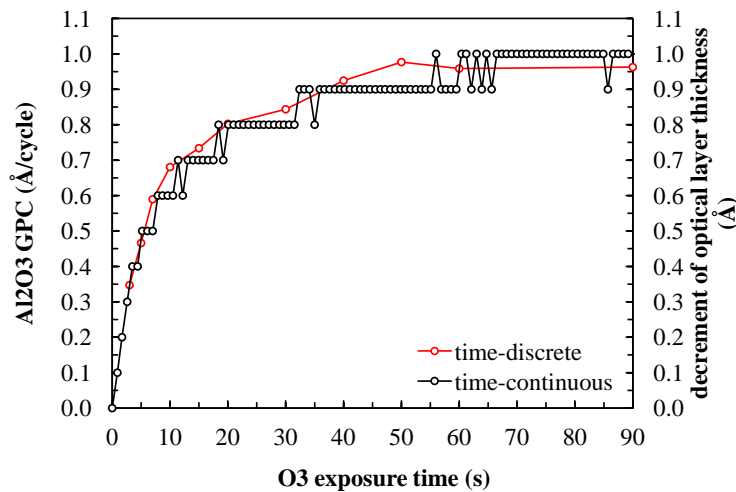


Figure 7.4.2 Time-discrete and time-continuous iSE measurements for shower head design of type II

7.4.3 Data evaluation

For all experiments done in this project, Al_2O_3 Cody-Lorentz oscillator material model for low absorbing and amorphous Al_2O_3 layer was chosen to describe the optical constants of film more precisely [Fujiwara 2007, p.172] [Ferlauto u. a. 2002]. Al_2O_3 layer was assumed to have isotropic, temperature and depolarization independent behaviour. Surface roughness was also neglected according to in-vacuo AFM measurements (see figure 8.3.9). A NTVE_JAW [from Herzinger u. a. 1998] material model for native SiO_2 was chosen. Also in order to get the information regarding the actual Si-surface temperature, Si_TEMP_JAW(Temp_Library) [proposed by Jellison and Modine] material model was selected from the software because it has the temperature as a fit parameter. A

relationship between the actual Si-surface and set point temperature has been plotted in figure 7.4.3 [more details in appendix and Junige u. a., p.2]. Figure 7.4.4 shows a difference between a set point temperature and the actual $\vartheta_{\text{Surface}}$ which was obtained by fitting in-situ SE data.

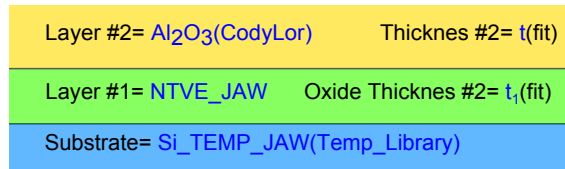


Figure 7.4.3 optical stack layer model for Al_2O_3 on Si substrate with native oxide

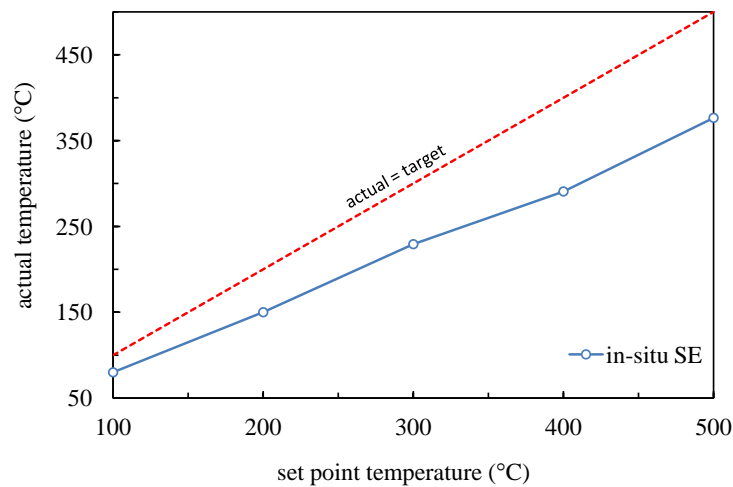


Figure 7.4.4 actual temperature versus target substrate temperature

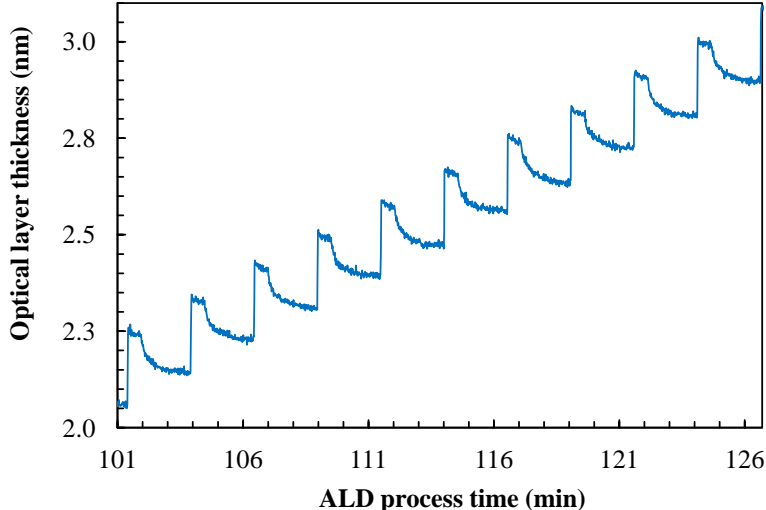
7.4.4 Post processing of data

Figure 7.4.5 a shows the evaluated optical layer thickness for 10 ALD cycles. Figure 7.4.5 b, indicates the start of each ALD cycle. Calculating the slope or so called first derivative of the thickness curve at each data point gives the film growth rate. Whenever the growth rate exceeds a specified threshold value (in this case 2 nm/min), the beginning of a new ALD cycle is indicated correspondingly and the ALD cycle index is incremented by 1 as shown in figure 7.4.5 c.

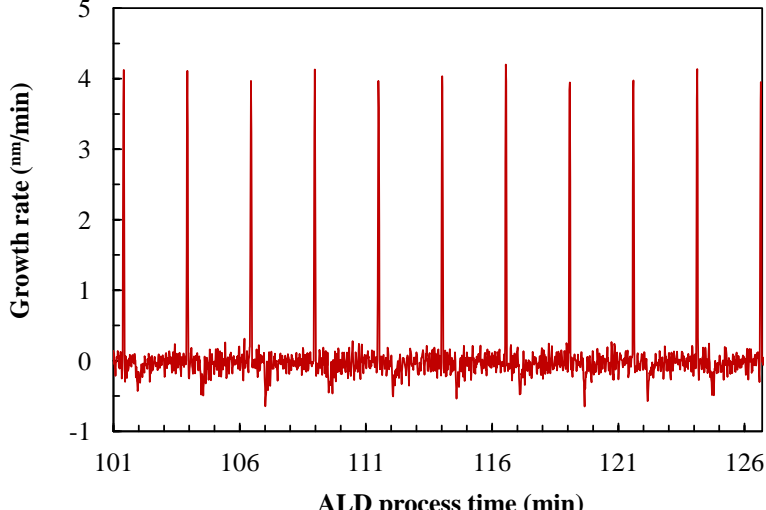
Each irtSE experiment in this report was performed with 100 ALD cycles. But actually only last 10 ALD cycles of the homogeneous growth region were superimposed to obtain one fine averaged optical layer thickness curve for progression of one ALD characteristic curve. Averaging reduces some random errors that will be described in section 7.4.5. This ALD averaged ALD characteristic curve was used in all other data evaluation processes.

Figure 7.4.5 Schematic representation of 10 ALD cycles

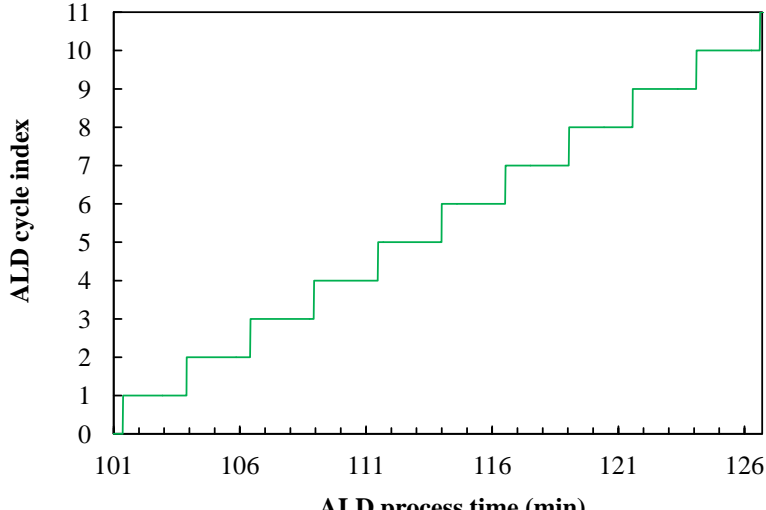
a optical layer thickness of Al₂O₃ for continuous 10 ALD cycles with ALD process time



b growth rate versus ALD process time



c ALD cycle index versus ALD process time



Kinetic ALD characteristic curve attributes were studied by analysing the time-resolved results obtained from irtSE. As described before, an averaged ALD characteristic curve was obtained from 10 continuous cycles in order to minimize the noise occurred while acquisition of data. ALD characteristic curve attributes; M_{ads} was evaluated by taking a maximum value in an ALD characteristic curve, L_{rem} was evaluated by subtracting the minimum value from blue region in figure 3.5.1 from M_{ads} and GPC was the global minima of fourth step in a complete ALD cycle (i.e. second Ar purge region in figure 3.5.1). In order to obtain the kinetic parameter of O_3 reaction step ' K_{O_3} ' more accurately, a fitting function shown below was chosen

$$y = y_0 + A \cdot \exp(-K_{O_3} t) \quad (7.1)$$

where 't' is ALD process time, y_0 and A are fit constants. This is an inbuilt exponential decay function available in mathematical software called OriginPro (Version 9.0). The fitting was only done for the blue region in figure 3.5.1 which indicates the O_3 reaction step.

7.4.5 Sources of errors in SE

In general, there are always three broad categories of errors present in any analytical or measurement technique. These are hardware related errors, errors due to software or optical model and human errors. Generally in ellipsometry, errors caused by some failures in hardware, misalignment of optical elements, sample misalignments, substrate backside reflections etc. can propagate into the final parameter evaluations and must be taken into account. Software errors can be caused due to wrong algorithms in software, errors in model [J.A. Woollam Co. 2011, p. 9-325 - 9-326] etc. Assuming, the software uses an accurate theory behind ellipsometry, this kind of errors can not be reduced without the help of manufacturer's support. Human errors arise due to lack in knowledge or unintentional mistakes caused during evaluations and can be minimised by increasing the conceptual knowledge and experience.

In SE, hardware errors are either random or systematic. Random hardware errors are generally small, because SE measures intensity ratios. Hence, errors caused due to fluctuations in the absolute light lamp intensity or incomplete collection of light from the sample do not result in increase in the error [Tompkins u. Irene 2005, p.474]. Consequently, SE measurements are very precise. This precision can be increased by averaging of several experiments done under similar process conditions, and then calculating the standard deviation (SD) and mean [Tompkins u. Irene 2005, p.266] (i.e. increasing the integration time). Thus making in-situ SE measurements more precise.

Systematic hardware errors are probably the most important, but hard to identify. They are bigger in magnitude and are more significant as compared to random hardware errors. Systematic errors occur due to misalignment of optical elements, calibration drifts, angle of incidence and depolarization effects and are SE equipment dependent. One way to minimize these errors is to incorporate some parameters as fitting parameters like angle of incidence offsets, window effects and depolarization effects [Tompkins u. Irene 2005, p.475].

In detail, misalignment of optical elements can cause errors in measuring (Ψ , Δ) values. Errors in Ψ can be due to misalignment in static or rotating elements like input polarizer, rotating compensator and analyzer (i.e. polarizer on detector side), respectively. In RCE type of configuration, error in Ψ can be minimized by performing measurements in high accuracy mode or by adding Ψ offset. While performing measurements in high accuracy mode, the analyzer spins to two different positions and eliminates the error in Ψ . While performing fast acquisitions, systematic errors can be reduced by adding Ψ offset in model options during post-data evaluation. On the other hand, error in Δ can occur due to undesired material deposition on window glasses, or due to slight thermal drifts compared to system calibration conditions. Windows at the FHR-ALD-300 tool are purged with Ar continuously, in order to keep them free from any depositions and thus, minimizing the measurement error in Δ . Temperature drifts can be optically modelled by adding some offset in Δ [Johs 2000].

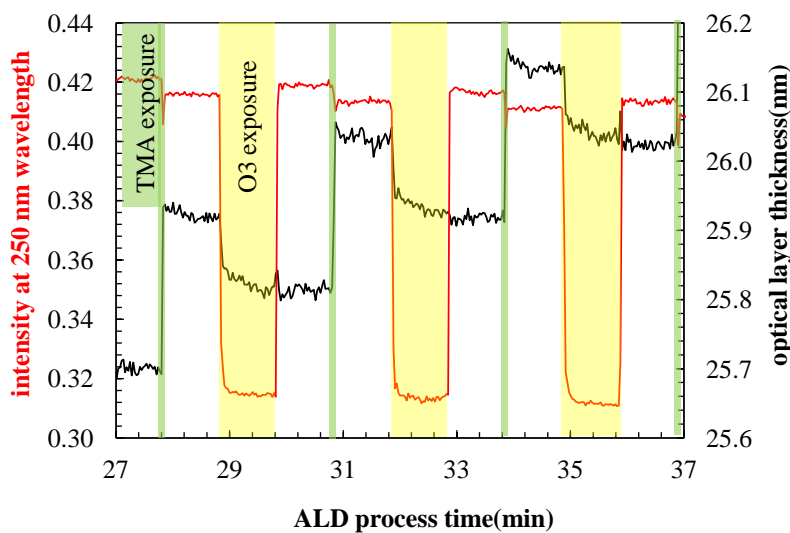


Figure 7.4.6 signal intensity of 250nm wavelength (red) and optical layer thickness (black) versus ALD process time

Other source of systematic error can occur due to improper selection in range of wavelengths. As one of our precursors was ozone. And ozone molecules absorb the light in ultraviolet range (wavelength below 300nm). It is shown in figure 7.4.6, where ozone and TMA exposure has been highlighted by yellow and green colours, respectively. The

red curve shows the drop in light intensity at 250nm wavelength, only at those moments when ozone was introduced in chamber. And black curve shows the change in optical layer thickness versus time. This curve is superimposed on the red curve to match the exact point of drop in the intensity curve. Thus one can be really assure that ozone was the real cause for this periodic intensity drop. Consequently, all experiments in this research project used a wavelength range from 300nm to 1690nm. This was important to reduce the MSE by factor 15% to 20%.

8 RESULTS AND DISCUSSION

8.1 INTRODUCTION

In general, the overall ALD process can be divided into two different growth regimes: the initial growth mechanism on heterogeneous starting substrate, followed by homogeneous film-by-film growth on a material itself [Puurunen 2005] [Soto 1991, p.2695]. Al_2O_3 has been grown on HF-etched silicon substrates, without creating a silicon-oxide interface, but with a slight inhibition [Nalwa 2002, p.131] [Delabie u. a. 2012, p.3]. In this report, the initial substrates used were c-Si with native oxide. As previous research has shown almost no incubation for Alumina growing on such hydroxylated silicon substrates [Nalwa 2002, p.131]. An ideal linear growth initialization was assumed in this report, and the results presented in the following sections focus on homogeneous linear film-on-film growth region.

In section 8.2, the kinetic ALD characteristic curves are studied by time-discrete iSE (as described in section 7.4.2) along with comparison of two gas shower head designs. This includes variation of the TMA exposure time, Ar purging time after TMA exposure, ozone exposure time and Ar purging time after ozone exposure, respectively. In section 8.3, the impact on characteristic ALD growth attributes and film properties by varying process parameters like total process pressure, Ozone flow and deposition temperature are investigated in more detail by time-continuous iSE.

8.2 KINETIC ALD CHARACTERISTIC CURVES

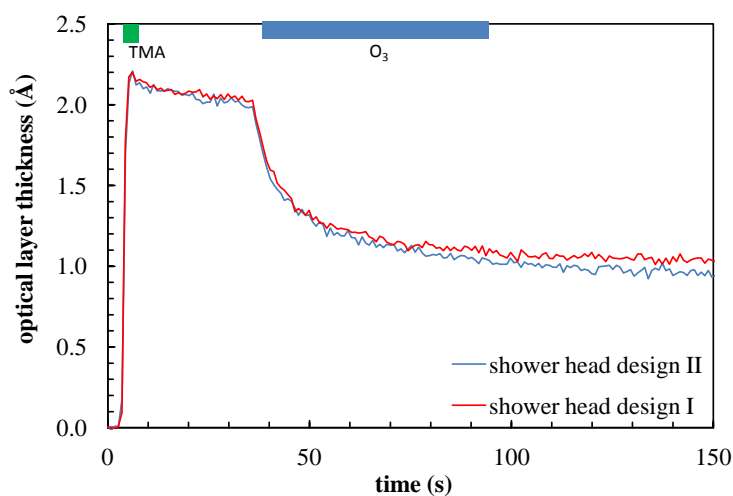


Figure 8.2.1 kinetic ALD characteristic curves for shower head design type I and II at deposition temperature of 150°C and total process pressure of 150 Pa

ALD characteristic curve is the curve that provides the information (for example in terms of optical thickness, frequency drop as revealed by irtSE and QCM, respectively) regarding each step (four steps of ALD cycle as described in section 3.2) of an ALD cycle. Figure 8.2.1 is a time-continuous iSE measurement and compares the ALD characteristic curve for both type I and type II shower head designs. Where green and blue highlighted portions show the TMA and ozone exposure times. Figure shows a small difference in O_3 exposure and Ar purge after behaviour O_3 exposure step for both shower head designs. However, each step in ALD characteristic curve is studied in detail with the help of exposure and purging time variations for both reactants, respectively.

8.2.1 TMA exposure

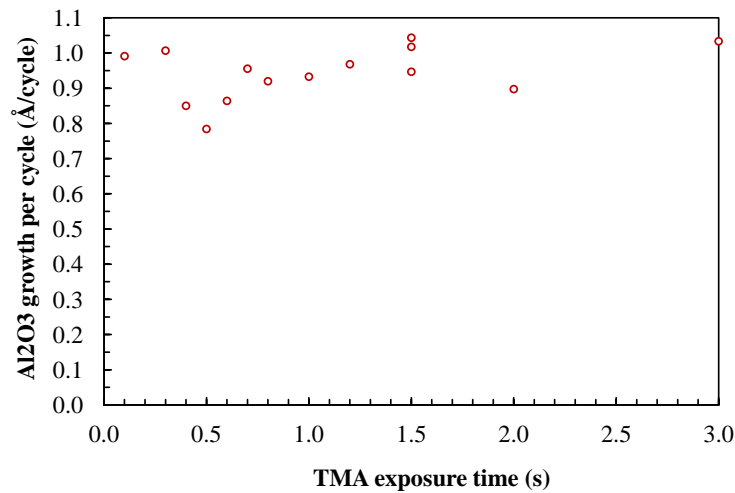


Figure 8.2.2 variation in TMA exposure time

First and foremost step of every Al_2O_3 ALD process from TMA and O_3 is the exposure of trimethylaluminium (as a first reactant). TMA exposure time was varied from 0.1 s to 3 s for a type I shower head design. A time-discrete irtSE measurement method was employed to study growth per cycle for each step variation and a TMA exposure time curve has been plotted in figure 8.2.2.

In figure 8.2.2, it can be seen that GPC tends to saturate right after 1.5 s of TMA exposure time. Thus a minimum amount of TMA dose needed is 1.5 s in order to have self-limited TMA adsorbed substrate surface.

The above experiments with same process conditions for shower head design of type II were not performed, and saturation of TMA after 1.5 s was assumed.

8.2.2 Argon purging after TMA exposure

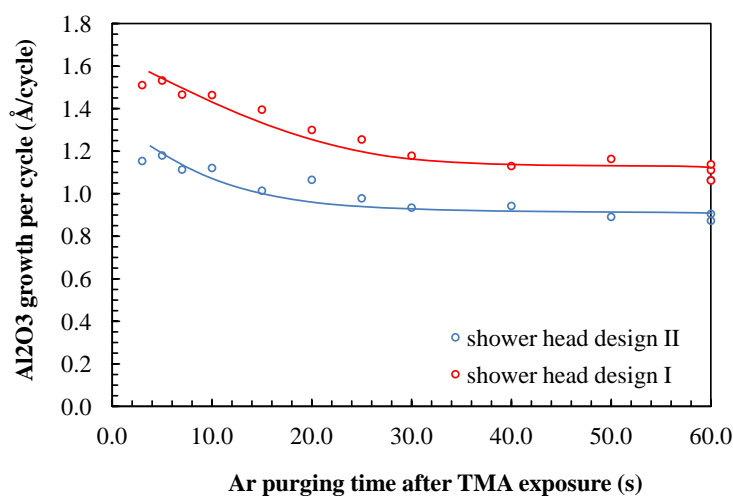


Figure 8.2.3 variation in Ar purging time after TMA exposure

Ar purging after TMA exposure is a necessary step to remove excessive TMA molecules and by-products from the process chamber. Thus leaving the substrate surface (with TMA adsorbates) ready for a second half-reaction with ozone. In figure 8.2.3, Ar purging after TMA exposure time curves have been plotted for shower head designs of type I and II.

A set of red data points shows the Argon purge variations were done with a type I shower head design installed in the chamber. It is found that the saturation point for type I shower head design was achieved after 30 s of Ar purging. For a type II shower head design this point is approximately 20 s. After these points of inflection, no significant change in growth per cycle has been seen and the curve tends to saturate beyond. It can be also seen that the Ar purging time less than these points of inflection tends to provide with GPC value more than 1 Å/cycle. Because the amount of Ar gas needed to purge all excessive surface molecules is too less. If the Ar purging times are too less, then it may cause overlapping of two reactants. Which may introduce a CVD like effect, that manifests as increased growth rate and thickness non-uniformities [Nalwa 2002, p.140].

In figure 8.2.3, the Al₂O₃ growth per cycle levels are significantly reduced in case of type II shower head design. Also the GPC levels after saturation point for type II shower head design are close to 1 Å/cycle. While in case of type I shower head design GPC values tends to settle around 1.2 Å/cycle. This can be due to more effective purging of gas channels inside the shower head, where residual precursor could have been concealed.

8.2.3 Ozone exposure

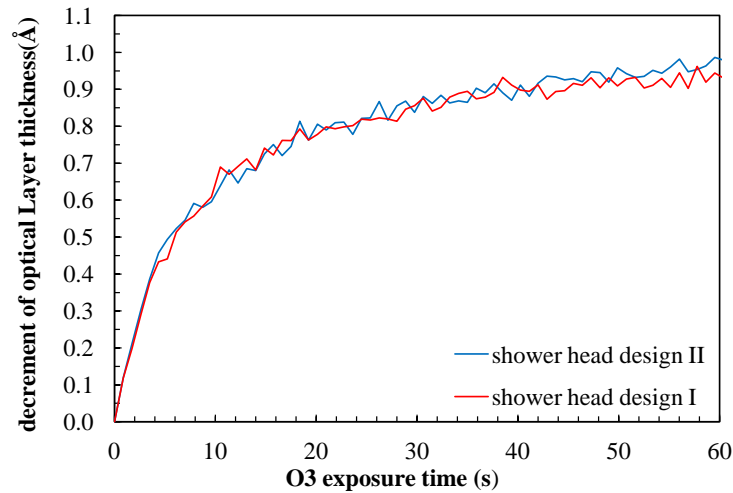


Figure 8.2.4 variation in O₃ exposure for both type of shower head designs - a time-continuous irtSE measurement

Ozone exposure completes the second half reaction and the Al₂O₃ layer is obtained. In figure 8.2.4, saturation curves of ozone for both shower head designs have been plotted from time-continuous irtSE. These curves are obtained by inverting the ozone exposure (growth decay portion in figure 8.2.1) from ALD characteristic curves for both type of shower head designs. The red and blue curves in the figure above is ozone exposure curve for shower head design I and II, respectively. For both shower head designs, the experiments were done at substrate temperature of 150°C and 150 Pa of total process pressure. These curves indicates the minimum amount of ozone exposure needed to have a completed reaction with all the TMA adsorbates on the surface. It can be seen that, the trend for saturation is almost comparable for both shower head designs. However, the blue curve shows a slight faster decay (also in figure 8.2.1) but this decay is small and can be neglected too. This means, the reaction of O₃ was not limited by the transportation of fresh O₃ molecules to the surface, but by reaction kinetics of the O₃ molecules with TMA adsorbate itself.

8.2.4 Argon purging after ozone exposure

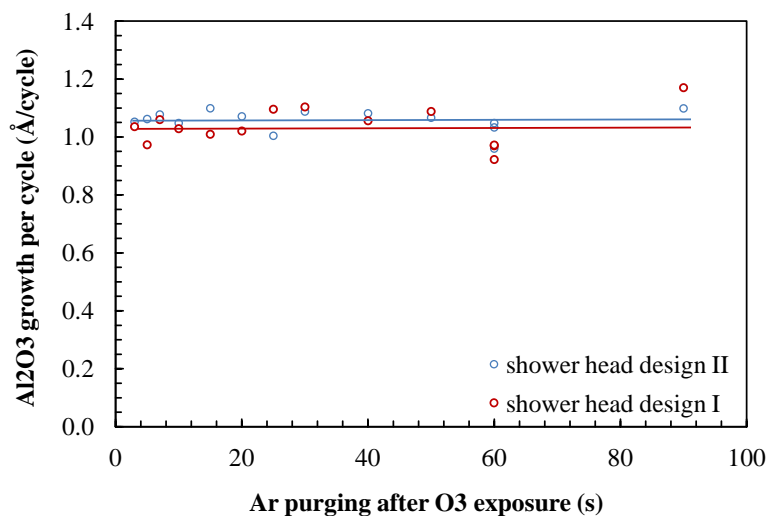


Figure 8.2.5 variation in Ar purging time after ozone exposure

This Ar purging step is necessary to remove the reaction by-products and the excessive ozone molecules from the chamber. Reaction by products being ethyne and other formate complexes [Goldstein u. a. 2008; Kim u. a. 2006].

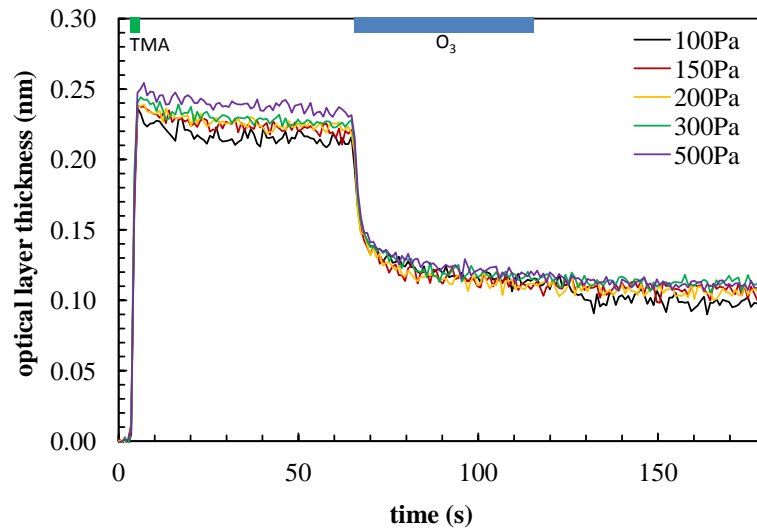
For both type of shower head designs, all the experiments and chamber conditions were unchanged thus ensuring the comparable results. Experimental conditions being the flow of gases, temperature of 150°C and chamber pressure (200 Pa). Figure 8.2.5 shows that GPC level is around 1Å/cycle for both shower head designs. Also there is almost no change in growth per cycle with varying Ar purging time after ozone exposure for both type of shower head designs, indicating a very fast removal of O₃ out of the reaction zone.

8.3 IMPACT OF PROCESS PARAMETERS ON CHARACTERISTIC ALD GROWTH ATTRIBUTES AND FILM PROPERTIES

8.3.1 Total process pressure

Figure 8.3.1 variation in total process pressure

a ALD characteristic curves for Al_2O_3 depositions at different pressures



b ALD characteristic curve attributes for Al_2O_3 depositions at different pressures

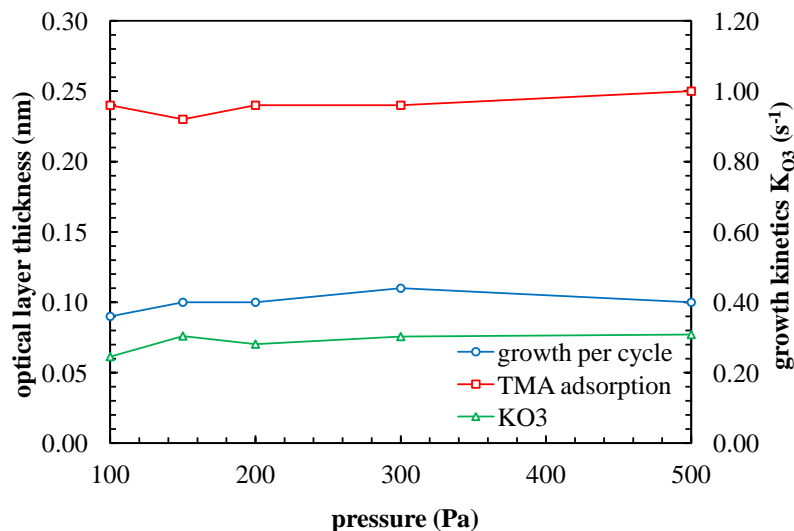


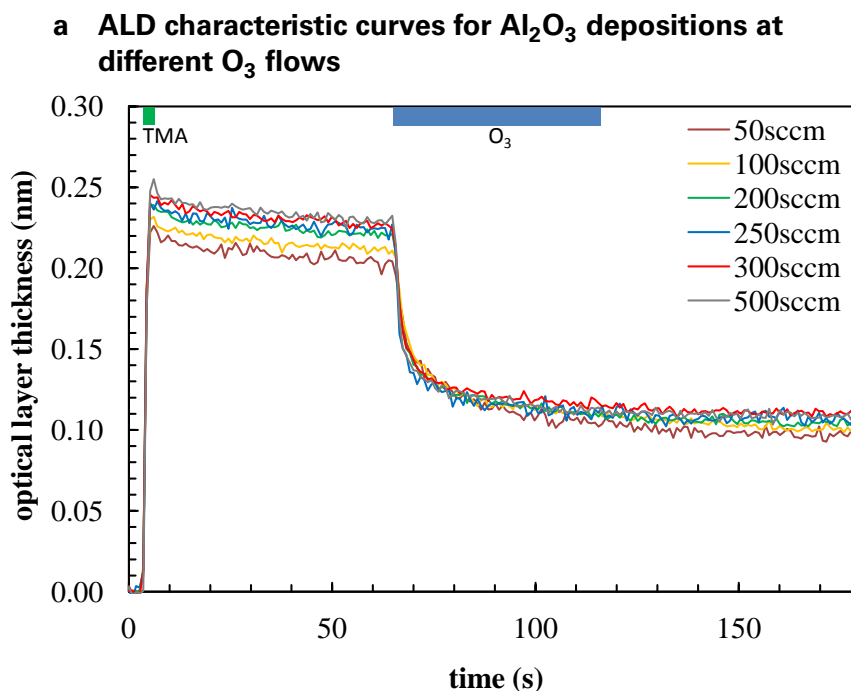
Figure 8.3.1a shows the change in optical layer thickness versus the ALD cycle time at different pressures. Each colored curve in a plot denotes one Averaged ALD characteristic curve obtained from 10 cycles that was described before in section 3.5. From this

figure it can be interpreted that, the chamber pressure has not much effect on various attributes of the process. All the curves are approximately superimposed on each other.

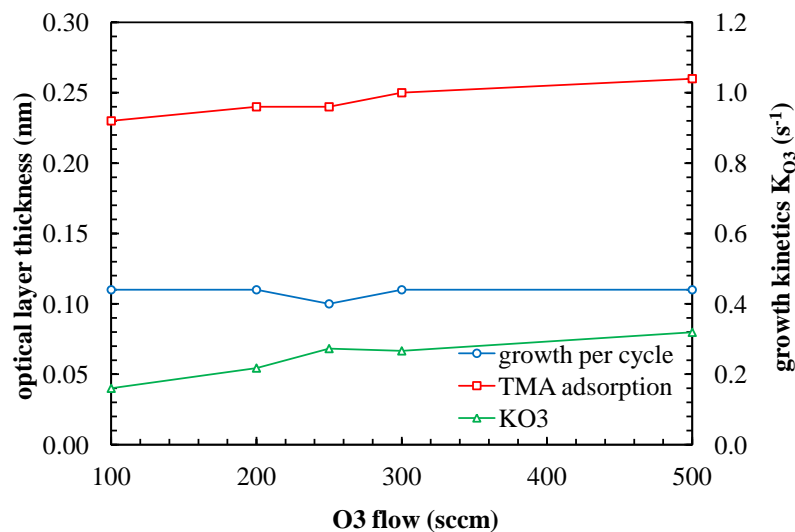
Figure 8.3.1b, elucidates the dependency of pressure on the various attributes of an ALD characteristic curve like TMA adsorption, GPC and growth kinetics ' K_{O_3} '. It can be seen from this figure that, the effect of total process pressure on GPC is nearly constant. However, the TMA adsorption seems to increase by very little amount. With increase in pressure there can be more adsorption on the substrate surface because increase in pressure can increase the kinetic energy of molecules that may facilitate TMA adsorption on the surface. Anyhow this change is so little and can be neglected too. Figure also shows that variation in total process pressure has no significant effect on growth kinetics ' K_{O_3} '. However, a little increase in growth kinetics can be favoured with the help of same reason given above. At low total process pressures (100 Pa, 150 Pa), all attributes have the minimum value among all values at various other pressures. This can be supported by an argument that, at low process pressure TMA and ozone molecules have less kinetic energy. Therefore showing minimum amount of TMA adsorption and slow reaction with ozone molecules, respectively.

8.3.2 Ozone flow

Figure 8.3.2 variation in O_3 flow



b ALD characteristic curve attributes for Al_2O_3 depositions at different O_3 flows



The ozone flow was varied manually by setting the needle valve position attached next to the ozone MFC (see table A.2 in appendix). The figure 8.3.2a, depicts the dependency of optical layer thickness for various ALD characteristic curves at different O_3 flows.

The ozone flow was varied from 50 sccm upto 500 sccm as shown in table B.1. The figure depicts the small trend while moving from 50 sccm to 500 sccm. This dependency was studied thoroughly with the help of figure 8.3.2b. It can be seen, that growth per cycle is not much changed with increase in ozone flow. And it was same with the case of TMA adsorption. However, the only thing that has been affected was the growth kinetics ' K_{O_3} '. A small trend was found in ' K_{O_3} ' and it seems that growth kinetics tends to depend on the ozone flow. With increase in ozone flow from 50 sccm to 500 sccm the growth kinetics was increased from 0.14 sec^{-1} upto 0.32 sec^{-1} .

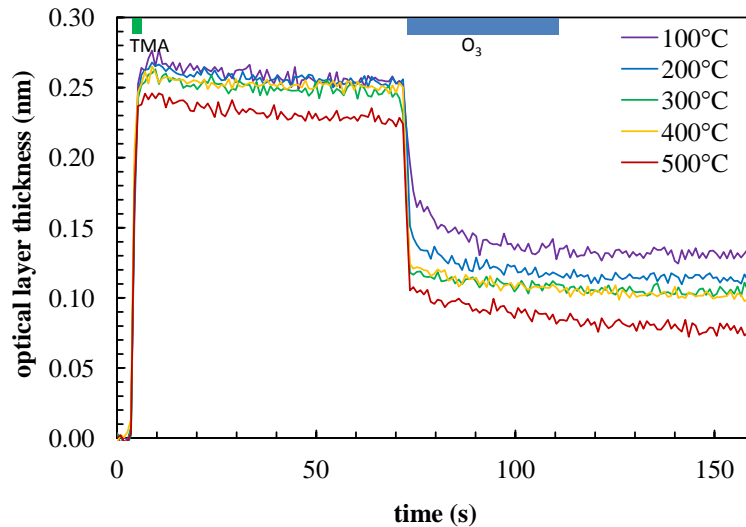
This means that with increase in ozone flow the reaction with TMA adsorbate is faster and it keeps on increasing but the GPC was not changed much. More precisely, in this figure the decay part (blue part in figure 3.5.1) of the whole ALD cycle tends to decrement faster and thus attaining the GPC value much more quicker in higher flow rates than in the case of low flow rates. This can also lead to stabilization of particular GPC level much quicker for higher O_3 flow rates.

Also it might be possible that, setting higher ozone flow rate can affect the ozone saturation curve. But we did not perform that experiment and that might be executed in future. The discussion done in this section is in favor with [Nalwa 2002, p.140] which states that growth rate per cycle may be increased by increasing exposure time but not by increasing the precursor flux [Ozeki 1992][Jeong u. a. 1989][Ritala u. a. 1993].

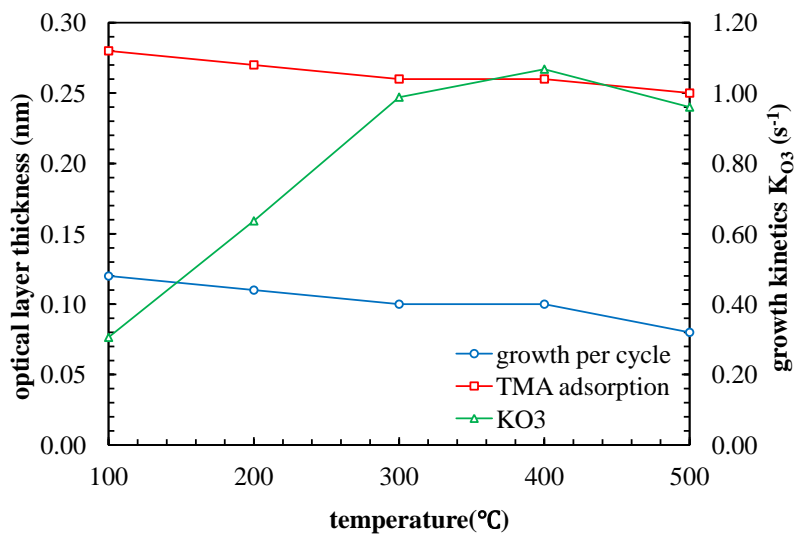
8.3.3 Deposition temperature

Figure 8.3.3 variation in deposition temperature

a ALD characteristic curves for Al_2O_3 depositions at different deposition temperatures



b ALD characteristic curve attributes for Al_2O_3 depositions at different deposition temperatures



The most important parameter among all ALD process parameters is the temperature that relies with results in [Yun 1997, p.2997]. Figure 8.3.3 shows that the deposition temperature was varied from 100°C to 500°C (see table B.1). From the figure 8.3.3a, it can be seen that an individual ALD characteristic curve tends to deviate from each other very significantly. As it was not the case for total process pressure and ozone flow variations, where all ALD characteristic curves superimpose on each other.

All attributes of ALD characteristic curve seems to be affected by deposition temperature. This can be realized better with the help of figure 8.3.3b where the TMA adsorption has been decreased slightly with increase in temperature but this dependency is small and can be neglected. It can be asserted that at higher temperatures, the TMA molecules have more kinetic energy and start to leave the surface. Hence in this report, we can neglect the effect of temperature on the TMA adsorption.

As compare to other process parameters GPC has been affected most by temperature and this change is not small to neglect. In figure 8.3.3b, the GPC value has been reduced from 1.3 Å per cycle to 0.8 Å per cycle. This result was in accordance with [Puurunen 2005], in which the decrease in GPC with increase in temperature was shown. This might be the case where at high temperatures, the newly formed aluminium oxide atoms do the self alignment and arrange into closely packed layers. It can also be the case where at higher temperatures, ozone molecules dissociates and forms the more reactive radicals and might had started etching the newly formed Al_2O_3 layer or can be some other reason or combination of many postulates.

Also, the effect of temperature on growth kinetics ' K_{O_3} ' has been shown in figure 8.3.3b, where ' K_{O_3} ' tends to show some increase with increase in temperature upto 300°C. Above this point the O_3 reaction kinetics was stabilized or slightly decreased for 500°C. Thus from this figure it can be said that optimum temperature would be around 300°C where the GPC is also close to 1 Å per cycle and the growth kinetics ' K_{O_3} ' is also the highest attaining the value of 1 s^{-1} .

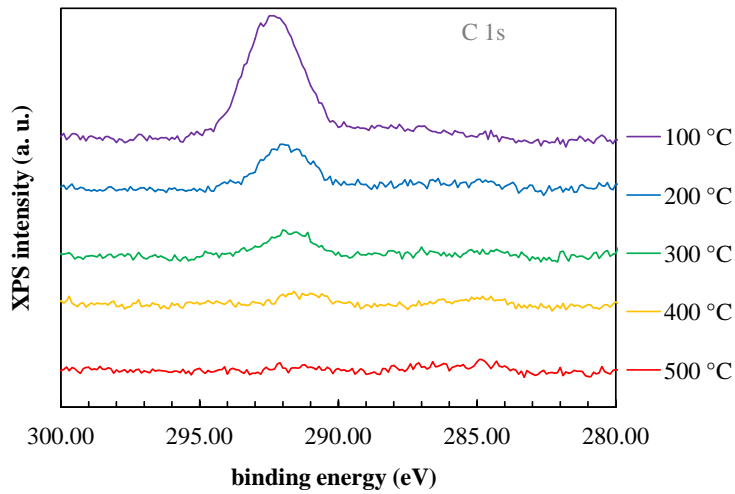
XPS analysis

To understand better the effect of deposition temperature on ALD characteristic curve attributes, a quantitative analysis by X-ray photoelectron spectroscopy was done. It provides the information on the composition of elements that are present on the surface of deposited material. In order to perform qualitative analysis, the sample substrate was transferred to the in-vacuo XPS analysis directly, thus keeping it unaltered. In this way, it was very promising to do the chemical composition analysis of the actual material deposited.

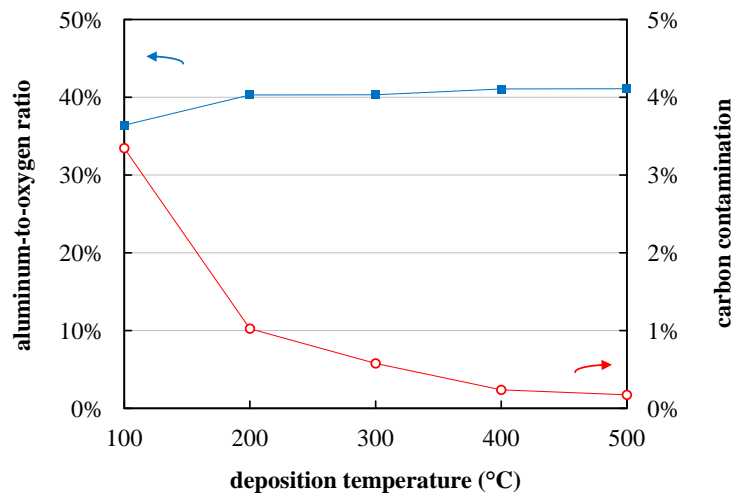
Figure 8.3.4a depicts the effect of deposition temperature on carbon (C1s peak) contaminations. For 100°C, it can be seen that the peak is approximately at 292 e.V and is of maximum area as compare to all peaks at other temperatures. For higher temperatures, the area under the peak was reduced by a significant value.

Figure 8.3.4 XPS analysis at different deposition temperature

a XPS intensity peaks for carbon (1s) at various deposition temperatures



b carbon contamination and aluminum to oxygen ratio at various deposition temperatures



This can be better seen in figure 8.3.4b, where right horizontal axis shows the change of carbon contamination level (at percentage) with varied deposition temperatures. At 100°C a carbon contamination level is maximum (3.2%). This value has suddenly dropped to 1% for 200°C. This drop in itself is large enough to show the improvement in Al_2O_3 film quality over temperature. Carbon contaminations can still be seen decreasing with rise in temperature, contamination level of almost 0.6% at 300°C to 0.3% approximately for 400°C and finally below the detection limit at 500°C. The resulting decrease in carbon contamination level with increase in deposition temperature is in favour of [Yun 1997].

In addition, the figure 8.3.4b also shows the effect of temperature variation on aluminium

to oxygen ratio. With increase in temperature, the aluminium to oxygen ratio was almost constant around 40%. Being minimum of approximately 38% only for 100°C. This aluminium to oxygen ratio is close to the ideal case, where expected Al:O ratio is 40:60. Above all experiments were done at 200 Pa pressure with 100 cycles of ALD process and 5 seconds of TMA exposure, 60 seconds of Ar purging time after TMA exposure, 30 seconds of ozone exposure and 60 seconds of last Ar purge. With 75, 2000, 250 and 2000 sccm of respective gas flows.

AFM analysis

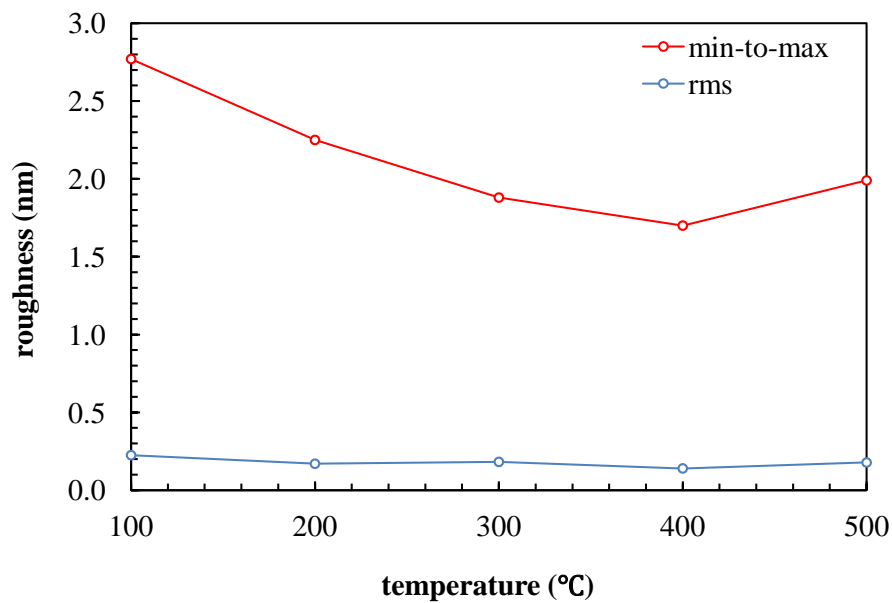


Figure 8.3.5 effect of temperature on surface roughness

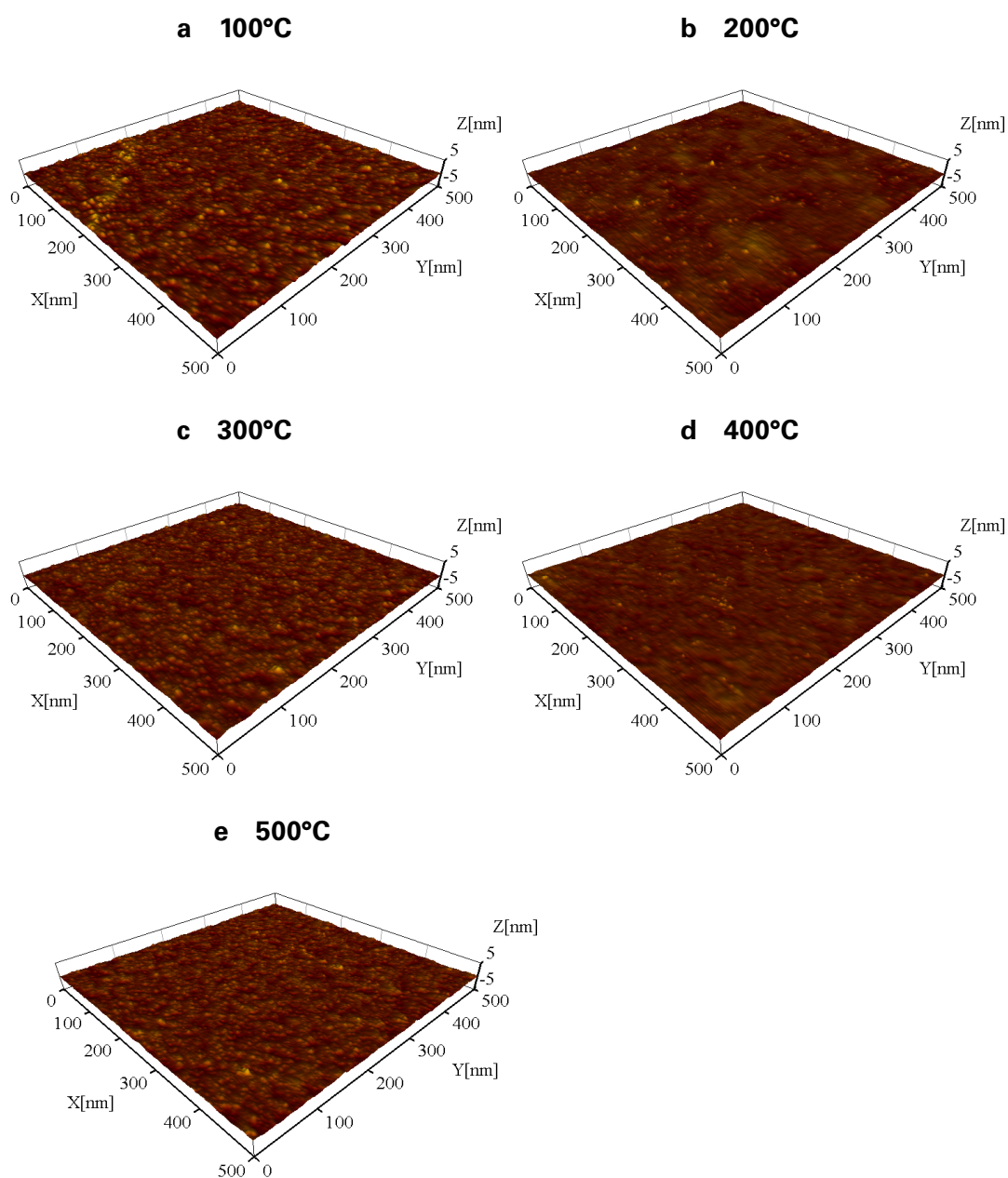
The final surface analysis technique used was an AFM for all temperature varied samples. The samples were analyzed in an area of 500nm by 500nm. Two kinds of roughness (min-to-max and rms) were evaluated. The min-to-max roughness is maximum z value plus the minimum z (tip position in z-direction) value.

Figure 8.3.5, shows an effect of substrate temperature on the surface (rms and min-to-max) roughness. This figure shows that temperature has almost no or little effect on rms roughness because it is pretty low approximately 0.2nm and stays almost constant. Nevertheless, peak roughness cannot be left unnoticed, the peak roughness seems to show some trend with temperature and the value has been changed from 2.8nm for 100°C to 1.7nm for 400°C. Then min-to-max roughness was increased again for 500°C to value 2nm approximately.

Figure 8.3.6 a) shows a 3-D plot of a aluminium oxide surface that was grown at 100°C

deposition temperature. The surface can be seen as various color spots, dark being the pits and light color means peaks. Other sub figures 8.3.6 b), c), d) and e) are for 200°C, 300°C, 400°C and 500°C deposition temperatures, respectively. 3-D plots, describe the surface impressions and depressions that are actually present on the sample surface. Each 3-D plot provides a topography of grown Al_2O_3 surface.

Figure 8.3.6 AFM topography after 100 Al_2O_3 ALD cycles at different temperatures

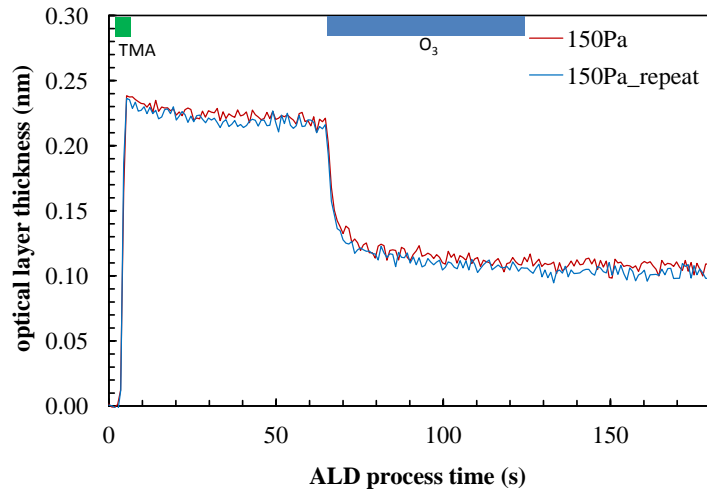


8.4 REPRODUCIBILITY

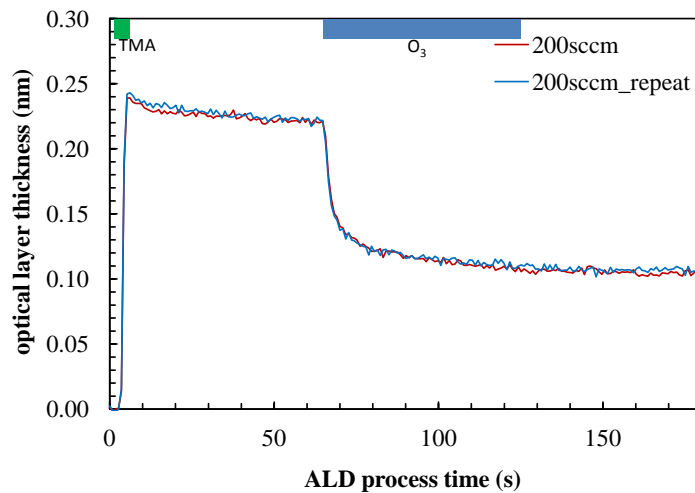
In order to check the repeatability of the developed ALD process, figure 8.4.1, shows reproduced ALD characteristic curves for two process conditions. Both curves, red and blue (being repeated) in each sub-figure overlap each other almost perfectly, denoting the reliability and reproducibility of the process, when performed again in same process conditions.

Figure 8.4.1 reproduced ALD cycle curves

a reproduced ALD cycle curve at 150Pa and 250 sccm of O₃ flow



b reproduced ALD cycle curve at 150Pa and 200 sccm of O₃ flow



9 CONCLUSIONS AND OUTLOOK

In summary this research project, the capability of an in-situ SE to measure various thin film parameters was demonstrated and refined. The in-situ measurements from iSE are very effective while describing the various film attributes like temperature, thickness, etc. Various ALD characteristic attributes like TMA adsorption, ligand removal, growth kinetics ' K_{O_3} ', growth per cycle have been studied in variation of exposure and purge times, deposition temperature, total process pressure and ozone flow. Also the performance of two shower head designs was compared. ALD characteristic curves for all four steps have been plotted and studied individually. Saturation of TMA adsorption was found after 1.5 seconds. Saturation point for Argon purge time after TMA exposure was found to be 20 seconds and 30 seconds for type II and type I shower head designs, respectively. Also it was noticed that in case of type II shower head design the GPC levels have reduced approximately by 25% as compare to GPC levels for type I shower head design. In case of type II shower head design the GPC level after saturation was close to 1 Å per cycle. For ozone exposure time, saturation takes place around 55 seconds for both shower head designs. After installing a new shower head design, there was no significant improvement found in the performance of Argon purge time followed by ozone exposure.

It has been found that the effect of substrate temperature on the various ALD cycle parameters is most substantial than any other ALD process parameter variations. Temperature has affected almost all ALD characteristic curve attributes (TMA adsorption, growth kinetics K_{O_3} , GPC, chemical composition and surface roughness). With increase in temperature, the carbon contaminations percentage levels were reduced to great extent. At the same time the aluminum to oxygen ratio was fairly constant for temperatures above 200°C. Min-to-max and rms roughness have been measured with the help of non-contact AFM method. And it was found that rms roughness stays at one level with unnoticeable change. While the min-to-max roughness minimized for temperature around 400°C to 500°C.

In a nutshell, it can be said that type II shower head design performs better than the type I shower head design. And the temperature was the major factor influencing the various attributes of ALD characteristic curve. Based on this research, I would suggest the optimized parameters for Al_2O_3 ALD process from TMA and Ozone (in ALD-300 tool from FHR anlagenbau GmbH with shower head type II installed in it) with 200Pa total process pressure, 300°C set point temperature and 250 sccm of ozone flow. A pulsing sequence of 1.5 s, 20s, 30 s and 10 s for TMA exposure, purge, O_3 exposure and purge, respectively, to produce carbon-free and smooth Al_2O_3 films.

ALD is very promising technique to deposit ultra thin and high quality films. With miniaturization according to need of future technologies, the quality has become of prime importance over speedy manufacturing. Methods for deposition and research of many more materials have been pipelined into researchers queue. Therefore in future, the

use of ALD technology is very promising. The results of this project can be incorporated and same methodology can be applied to study other materials like metals, nitrides and dielectrics. Moreover, this research can be broadened by studying the initial phase of deposition and also by studying the electrical properties like leakage current and breakdown voltage of deposited Aluminum oxide.

REFERENCES

Andrade 1985

ANDRADE, Joseph D.: *Surface and Interfacial Aspects of Biomedical Polymers: Volume 1 Surface Chemistry and Physics*. Boston and MA : Springer US, 1985. – ISBN 978–1–4684–8610–0

Aspnes u. Hauge 1976

ASPNES, D. E. ; HAUGE, P. S.: Rotating-compensator/analyzer fixed-analyzer ellipsometer: Analysis and comparison to other automatic ellipsometers. In: *Journal of the Optical Society of America* 66 (1976), Nr. 9, S. 949

B. Johs u. a. 1999

B. JOHS ; J. A. WOOLLAM ; C. HERZINGER ; J. HILFIKER ; R. SYNOWICKI ; C. BUNGAY: Overview of Variable Angle Spectroscopic Ellipsometry (VASE), Part II: Advanced Applications. (1999), S. 29–58

Bernardi u. a. 2004

BERNARDI, M. I. B. ; CRISPIM, S. C. L. ; MACIEL, A. P. ; SOUZA, A. G. ; CONCEICAO, M. M. ; LEITE, E. R. ; LONGO, E.: Synthesis and characterization of Al₂O₃/Cr₂O₃ - based ceramic pigments. In: *Journal of Thermal Analysis and Calorimetry* 75 (2004), Nr. 2, S. 475–480. <http://dx.doi.org/10.1023/B:JTAN.0000027135.04033.e8>. – DOI 10.1023/B:JTAN.0000027135.04033.e8. – ISSN 1388–6150

Binnig u. Quate 1986

BINNIG, G. ; QUATE, C. F.: Atomic Force Microscope. In: *Physical Review Letters* 56 (1986), Nr. 9, S. 930–933

cambridge nanotech July

CAMBRIDGE NANOTECH: *Cambridge NanoTech ALD tutorial*. <http://www.cambridgenanotechald.com/atomic-layer-deposition-overview.html>. Version: July 2011

Dale E. Morton u. a. 2002

DALE E. MORTON ; BLAINE JOHS ; JEFF HALE: Optical Monitoring of Thin-films Using Spectroscopic Ellipsometry. In: *Society of Vacuum Coaters* (2002)

Delabie u. a. 2012

DELABIE, Annelies ; SIONCKE, Sonja ; RIP, Jens ; ELSHOCHT, Sven van ; POURTOIS, Geoffrey ; MUELLER, Matthias ; BECKHOFF, Burkhard ; PIERLOOT, Kristine: Reaction mechanisms for atomic layer deposition of aluminum oxide on semiconductor substrates. In: *Journal of Vacuum Science & Technology A: Vacuum, Surfaces, and Films* 30 (2012), Nr. 1, S. 01A127. <http://dx.doi.org/10.1116/1.3664090>. – DOI 10.1116/1.3664090. – ISSN 07342101

Elliott u. a. 2006

ELLIOTT, S. D. ; SCAREL, G. ; WIEMER, C. ; FANCIULLI, M. ; PAVIA, G.: Ozone-Based Atomic Layer Deposition of Alumina from TMA: Growth, Morphology, and Reaction Mechanism. In: *Chemistry of Materials* 18 (2006), Nr. 16, S. 3764–3773. <http://dx.doi.org/10.1021/cm0608903>. – DOI 10.1021/cm0608903. – ISSN 0897–4756

Ferlauto u. a. 2002

FERLAUTO, A. S. ; FERREIRA, G. M. ; PEARCE, J. M. ; WRONSKI, C. R. ; COLLINS, R. W. ; DENG, Xunming ; GANGULY, Gautam: Analytical model for the optical functions of amorphous semiconductors from the near-infrared to ultraviolet: Applications in thin film photovoltaics. In: *Journal of Applied Physics* 92 (2002), Nr. 5, S. 2424

Fujiwara 2007

FUJIWARA, Hiroyuki: *Spectroscopic ellipsometry: Principles and applications*. Chichester and England and Hoboken and NJ : John Wiley & Sons, 2007. – ISBN 9780470060186

Goldstein u. a. 2008

GOLDSTEIN, David N. ; MCCORMICK, Jarod A. ; GEORGE, Steven M.: Al₂O₃ Atomic Layer Deposition with Trimethylaluminum and Ozone Studied by in Situ Transmission FTIR Spectroscopy and Quadrupole Mass Spectrometry. In: *The Journal of Physical Chemistry C* 112 (2008), Nr. 49, S. 19530–19539. <http://dx.doi.org/10.1021/jp804296a>. – DOI 10.1021/jp804296a. – ISSN 1932–7447

Gross u. a. 2009

GROSS, L. ; MOHN, F. ; MOLL, N. ; LILJEROTH, P. ; MEYER, G.: The Chemical Structure of a Molecule Resolved by Atomic Force Microscopy. In: *Science* 325 (2009), Nr. 5944, S. 1110–1114. <http://dx.doi.org/10.1126/science.1176210>. – DOI 10.1126/science.1176210. – ISSN 0036–8075

H. Suzuki u. a. 1989

H. SUZUKI ; N. FUJIMAKI ; H. TAMURA ; T. IMAMURA ; S. HASUO: A 4K Josephson memory - Magnetics, IEEE Transactions on. (1989)

Hans sundstrom 2005

HANS SUNDSTROM, M. I.: Ozone as the Oxidizing Precursor in Atomic Layer Deposition. (2005)

Hasuo 1992

HASUO, S.: High quality niobium Josephson junction for ultrafast computers. In: *Thin Solid Films* 216 (1992), Nr. 1, S. 21–27. [http://dx.doi.org/10.1016/0040-6090\(92\)90862-6](http://dx.doi.org/10.1016/0040-6090(92)90862-6). – DOI 10.1016/0040-6090(92)90862-6. – ISSN 00406090

Herzinger u. a. 1998

HERZINGER, C. M. ; JOHS, B. ; MCGAHAN, W. A. ; WOOLLAM, J. A. ; PAULSON, W.: Ellipsometric determination of optical constants for silicon and thermally grown silicon

dioxide via a multi-sample, multi-wavelength, multi-angle investigation. In: *Journal of Applied Physics* 83 (1998), Nr. 6, S. 3323

Himcinschi u. a. 2001

HIMCINSCHI, C. ; FRIEDRICH, M. ; MURRAY, C. ; STREITER, I. ; SCHULZ, S. E. ; GESSNER, T. ; ZAHN, D. R. T.: Characterization of silica xerogel films by variable-angle spectroscopic ellipsometry and infrared spectroscopy. In: *Semiconductor Science and Technology* 16 (2001), Nr. 9, S. 806–811

J. Spiegelman u. J. Sundqvist 2011

J. SPIEGELMAN ; J. SUNDQVIST: Comparison of Water Vapor to Ozone for growth of ALD Films Comparison of Water Vapor to Ozone for growth of ALD Films. In: *Gases&Instrumentation* (2011), S. 20–25

J.A. Woollam Co. 2011

J.A. WOOLLAM CO., Inc.: *Complete Ease: Data analysis Manual version (4.63)*. 645 M STREET, SUITE 102 LINCOLN, NE 68508-2243 USA : J.A. Woollam Co.,Inc., 2011

Jakschik u. a. 2003

JAKSCHIK, Stefan ; SCHROEDER, Uwe ; HECHT, Thomas ; KRUEGER, Dietmar ; DOLLINGER, Guenther ; BERGMAIER, Andreas ; LUHMANN, Claudia ; BARTHA, Johann W.: Physical characterization of thin ALD–Al₂O₃ films. In: *Applied Surface Science* 211 (2003), Nr. 1-4, S. 352–359. [http://dx.doi.org/10.1016/S0169-4332\(03\)00264-2](http://dx.doi.org/10.1016/S0169-4332(03)00264-2). – DOI 10.1016/S0169-4332(03)00264-2. – ISSN 01694332

Jellison 1998

JELLISON, JrG.E: Spectroscopic ellipsometry data analysis: measured versus calculated quantities. In: *Thin Solid Films* 313-314 (1998), Nr. 1, S. 33–39

Jeong u. a. 1989

JEONG, Weon G. ; MENU, E. P. ; DAPKUS, P. D.: Steric hindrance effects in atomic layer epitaxy of InAs. In: *Applied Physics Letters* 55 (1989), Nr. 3, S. 244

Joys 2000

JOYS, Craig M. Blaine D.; Herzinger H. Blaine D.; Herzinger: *Methods for uncorrelated evaluation of parameters in parameterized mathematical model equations for window retardance, in ellipsometer and polarimeter systems, United States Patent 6034777*. 2000

Junige u. a.

JUNIGE, Marcel ; GEIDEL, Marion ; KNAUT, Martin ; ALBERT, Matthias ; BARTHA, Johann W.: Monitoring atomic layer deposition processes in situ and in real-time by spectroscopic ellipsometry.

Kim u. a. 2002

KIM, J. B. ; KWON, D. R. ; CHAKRABARTI, K. ; LEE, Chongmu ; OH, K. Y. ; LEE, J. H.: Improvement in Al₂O₃ dielectric behavior by using ozone as an oxidant for the atomic layer deposition technique. In: *Journal of Applied Physics* 92 (2002), Nr. 11, S. 6739. <http://dx.doi.org/10.1063/1.1515951>. – DOI 10.1063/1.1515951. – ISSN 00218979

Kim u. a. 2003

KIM, Jaebum ; CHAKRABARTI, Kuntal ; LEE, Jinho ; OH, Ki-Young ; LEE, Chongmu: Effects of ozone as an oxygen source on the properties of the Al₂O₃ thin films prepared by atomic layer deposition. In: *Materials Chemistry and Physics* 78 (2003), Nr. 3, S. 733–738. [http://dx.doi.org/10.1016/S0254-0584\(02\)00375-9](http://dx.doi.org/10.1016/S0254-0584(02)00375-9). – DOI 10.1016/S0254-0584(02)00375-9. – ISSN 02540584

Kim u. a. 2006

KIM, Seong K. ; LEE, Suk W. ; HWANG, Cheol S. ; MIN, Yo-Sep ; WON, Jeong Y. ; JEONG, Jaehack: Low Temperature (<100Å°C) Deposition of Aluminum Oxide Thin Films by ALD with O₃ as Oxidant. In: *Journal of The Electrochemical Society* 153 (2006), Nr. 5, S. F69. <http://dx.doi.org/10.1149/1.2177047>. – DOI 10.1149/1.2177047. – ISSN 00134651

Manchanda u. a. 2001

MANCHANDA, L. ; MORRIS, M.D ; GREEN, M.L ; DOVER, R.B van ; KLEMENS, F. ; SORSCH, T.W ; SILVERMAN, P.J ; WILK, G. ; BUSCH, B. ; ARAVAMUDHAN, S.: Multi-component high-K gate dielectrics for the silicon industry. In: *Microelectronic Engineering* 59 (2001), Nr. 1-4, S. 351–359. [http://dx.doi.org/10.1016/S0167-9317\(01\)00668-2](http://dx.doi.org/10.1016/S0167-9317(01)00668-2). – DOI 10.1016/S0167-9317(01)00668-2. – ISSN 01679317

Mizuguchi u. a. 2005

MIZUGUCHI, M. ; SUZUKI, Y. ; NAGAHAMA, T. ; YUASA, S.: Atomically flat aluminum-oxide barrier layers constituting magnetic tunnel junctions observed by in situ scanning tunneling microscopy. In: *Applied Physics Letters* 87 (2005), Nr. 17, S. 171909. <http://dx.doi.org/10.1063/1.2108121>. – DOI 10.1063/1.2108121. – ISSN 00036951

Nalwa 2002

NALWA, Hari S.: *Handbook of thin film materials*. San Diego : Academic Press, 2002. – ISBN 0125129092

Ozeki 1992

OZEKI, M.: Atomic layer epitaxy of III–V compounds using metalorganic and hydride sources. In: *Materials Science Reports* 8 (1992), Nr. 3, S. 97–146

Park u. a. 2003

PARK, Hong B. ; CHO, Moonju ; PARK, Jaehoo ; LEE, Suk W. ; HWANG, Cheol S. ; KIM, Jong-Pyo ; LEE, Jong-Ho ; LEE, Nae-In ; KANG, Ho-Kyu ; LEE, Jong-Cheol ; OH, Se-Jung: Comparison of HfO₂ films grown by atomic layer deposition using HfCl₄

and H₂O or O₃ as the oxidant. In: *Journal of Applied Physics* 94 (2003), Nr. 5, S. 3641

Patnaik 2003

PATNAIK, Pradyot: *Handbook of inorganic chemicals*. New York : McGraw-Hill, 2003 (McGraw-Hill handbooks). – ISBN 0070494398

Perrella 2004

PERRELLA, Andrew C.: *Ballistic Electron Transport in Aluminum Oxide*, Cornell University, Diss., 2004

Puurunen 2005

PUURUNEN, Riikka L.: Surface chemistry of atomic layer deposition: A case study for the trimethylaluminum/water process. In: *Journal of Applied Physics* 97 (2005), Nr. 12, S. 121301. <http://dx.doi.org/10.1063/1.1940727>. – DOI 10.1063/1.1940727. – ISSN 00218979

Ritala u. a. 1993

RITALA, Mikko ; LESKELA, Markku ; NIINISTO, Lauri ; HAUSSALO, Pekka: Titanium isopropoxide as a precursor in atomic layer epitaxy of titanium dioxide thin films. In: *Chemistry of Materials* 5 (1993), Nr. 8, S. 1174–1181

Schmidt u. a. 2008

SCHMIDT, D. ; STREHLE, S. ; ALBERT, M. ; HENTSCH, W. ; BARTHA, J.W: Top injection reactor tool with in situ spectroscopic ellipsometry for growth and characterization of ALD thin films. In: *Microelectronic Engineering* 85 (2008), Nr. 3, S. 527–533

Siah u. a. 2013

SIAH, S.C ; HOEX, B. ; ABERLE, A.G: Accurate characterization of thin films on rough surfaces by spectroscopic ellipsometry. In: *Thin Solid Films* 545 (2013), S. 451–457

Skoog 1985

SKOOG, Douglas A.: *Principles of instrumental analysis*. 3. Philadelphia : Saunders College Pub., 1985 (Saunders golden sunburst series). – ISBN 9780030012297

Soto 1991

SOTO, C.: The reaction pathway for the growth of alumina on high surface area alumina and in ultrahigh vacuum by a reaction between trimethyl aluminum and water. In: *Journal of Vacuum Science & Technology A: Vacuum, Surfaces, and Films* 9 (1991), Nr. 5, S. 2686

Tompkins u. Irene 2005

TOMPKINS, Harland G. ; IRENE, Eugene A.: *Handbook of ellipsometry*. Norwich and NY and Heidelberg and Germany : William Andrew Pub. and Springer, 2005. – ISBN 0815514999

Wagner u. Muilenberg 1979

WAGNER, C. D. ; MUILENBERG, G. E.: *Handbook of x-ray photoelectron spectroscopy: a reference book of standard data for use in x-ray photoelectron spectroscopy*. Physical Electronics Division, Perkin-Elmer Corp, 1979 <http://books.google.de/books?id=oY5TAAAAYAAJ>

Yeong Kwan Kim u. a.

YEONG KWAN KIM ; SEUNG HWAN LEE ; SUNG JE CHOI ; HONG BAE PARK ; YOUNG DONG SEO ; KWANG HYUN CHIN ; DONGCHAN KIM ; JAE SOON LIM ; WAN DON KIM ; KAB JIN NAM ; MAN-HO CHO ; KI HYUN HWANG ; YOUNG SUN KIM ; SEOK SIK KIM ; YOUNG WOOK PARK ; JOO TAE MOON ; SANG IN LEE ; MOON YONG LEE: Novel capacitor technology for high density stand-alone and embedded DRAMs. <http://dx.doi.org/10.1109/IEDM.2000.904332>. – DOI 10.1109/IEDM.2000.904332

Yun 1997

YUN, Sun J.: Dependence of atomic layer-deposited Al₂O₃ films characteristics on growth temperature and Al precursors of Al(CH₃)₃ and AlCl₃. In: *Journal of Vacuum Science & Technology A: Vacuum, Surfaces, and Films* 15 (1997), Nr. 6, S. 2993. <http://dx.doi.org/10.1116/1.580895>. – DOI 10.1116/1.580895. – ISSN 07342101

Zhong u. a. 1993

ZHONG, Q. ; INNISS, D. ; KJOLLER, K. ; ELINGS, V.B: *Fractured polymer/silica fiber surface studied by tapping mode atomic force microscopy*. <http://www.sciencedirect.com/science/article/pii/016725849390906Y>. Version: 1993

Zhu u. Park 2006

ZHU, J. ; PARK, C.: Magnetic tunnel junctions. In: *Materials Today* 9 (2006), Nr. 11, S. 36–45. [http://dx.doi.org/10.1016/S1369-7021\(06\)71693-5](http://dx.doi.org/10.1016/S1369-7021(06)71693-5). – DOI 10.1016/S1369-7021(06)71693-5. – ISSN 13697021

ACKNOWLEDGMENTS

The research studies reported in this project were carried out during the year 2012–2013 in the Institute of Semiconductors And Microsystems at university of Technology Dresden, Germany.

First, I owe my deepest gratitude to my supervisors, Dipl.-Ing. Marcel Junige and Dipl.-Ing. Martin Knaut for their invaluable contribution and help to this study. Marcel, without your guidance this work would not have been done. Both of you had always time for me and your rapid feedback concerning my ongoing project was just unbelievable. I had a great time during the complete year, working with you.

My special thanks go to my Professor Dr.rer.nat. Johann W. Bartha, for his valuable support and advice during this year in and outside of the laboratory. I would also like to appreciate Dr.–Ing. Matthias Albert for his advice and timely evaluation of my presentations. I owe warm thanks to Zulfija Ritter for her kind advice and help in AFM and ex-situ SE measurements.

III APPENDIX

A REFERENCE TEMPERATURES AND OZONE FLOW

The table A.1 shows the actual substrate temperature obtained after fitting the SE model parameters (temperature in Si_TEMP_JAW(Temp_Library)) and measured data in corresponding to set point temperatures. Set point temperature is the temperature of substrate heating plate. But the actual temperature is the temperature of substrate surface. There is a significant temperature difference between the substrate heating plate and the surface. This difference is due to loss in transfer of heat from heating plate to small coupons of substrate, where actual depositions had taken place.

Sr.No.	Set-point Temperature(°C)	Actual Temperature(°C)
1	100	80.00
2	200	150.00
3	300	229.32
4	400	290.73
5	500	376.50

Table A.1 actual substrate temperatures corresponding to set-point temperatures

Sr.No.	Oxygen flow (sccm)	Total chamber pressure(Pa)	Needle valve position	
			Oxygen(O ₂)	Ozone(O ₃)
1	50	9	0.20	1.13
2	100	12	1.07	2.05
3	200	17	1.12	3.05
4	250	19	1.7	3.175
5	300	21	2.05	4.05
6	500	28	3.09	6.05

Table A.2 O₂ and O₃ gas flows with their corresponding needle valve positions

B PROCESS PARAMETERS

Tables B.1, B.2, B.3, B.4 and B.5 show the variation in various process parameters. Various process parameters being total process pressure, deposition temperature, O₃ flow, and variation in TMA, Ar, O₃ exposure and purging times. All these variations have been shown in coloured text, while the rest of the process parameters being unaltered. Where t_{TMA} , t_{Ar_1} , t_{O_3} , t_{Ar_2} are the TMA exposure, Ar purge time after TMA exposure, O₃ exposure time and Ar purge time after O₃ exposure. All variations in table B.1, have been performed with type II shower head design installed. While the rest of the parameters were varied for both type I and type II shower heads installed in the chamber. But the t_{TMA} variations were only carried with type I shower head design.

Variation	Pressure(Pa)	O ₃ flow (sccm)	$\vartheta_{Substrate}$ (°C)	t_{TMA} (s)	t_{Ar_1} (s)	t_{O_3} (s)	t_{Ar_2} (s)
Pressure	100	250	100	1.5	60	30	60
	150	250	200	1.5	60	30	60
	200	250	300	1.5	60	30	60
	300	250	400	1.5	60	30	60
	500	250	500	1.5	60	30	60
Ozone	200	50	150	1.5	60	30	60
	200	100	150	1.5	60	30	60
	200	200	150	1.5	60	30	60
	200	250	150	1.5	60	30	60
	200	300	150	1.5	60	30	60
	200	500	150	1.5	60	30	60
Temperature	200	250	100	5	60	30	60
	200	250	200	5	60	30	60
	200	250	300	5	60	30	60
	200	250	400	5	60	30	60
	200	250	500	5	60	30	60

Table B.1 process parameter variations

Variation	Pressure(Pa)	O ₃ flow (sccm)	$\vartheta_{Substrate}$ (°C)	t_{TMA} (s)	t_{Ar_1} (s)	t_{O_3} (s)	t_{Ar_2} (s)
t_{TMA}	200	200	150	0.1	30	60	60
	200	200	150	0.3	30	60	60
	200	200	150	0.4	30	60	60
	200	200	150	0.5	30	60	60
	200	200	150	0.6	30	60	60
	200	200	150	0.7	30	60	60
	200	200	150	0.8	30	60	60
	200	200	150	1.0	30	60	60
	200	200	150	1.2	30	60	60
	200	200	150	1.5	30	60	60
	200	200	150	2.0	30	60	60
	200	200	150	3.0	30	60	60

Table B.2 variations in TMA exposure time

Variation	Pressure(Pa)	O ₃ flow (sccm)	$\vartheta_{\text{Substrate}}(^{\circ}\text{C})$	$t_{TMA}(\text{s})$	$t_{Ar_1}(\text{s})$	$t_{O_3}(\text{s})$	$t_{Ar_2}(\text{s})$
t_{Ar_1}	200	200	150	1.5	3	60	60
	200	200	150	1.5	5	60	60
	200	200	150	1.5	7	60	60
	200	200	150	1.5	10	60	60
	200	200	150	1.5	15	60	60
	200	200	150	1.5	20	60	60
	200	200	150	1.5	25	60	60
	200	200	150	1.5	30	60	60
	200	200	150	1.5	40	60	60
	200	200	150	1.5	50	60	60
	200	200	150	1.5	60	60	60

Table B.3 variations in Ar purge time after TMA exposure

Variation	Pressure(Pa)	O ₃ flow (sccm)	$\vartheta_{\text{Substrate}}(^{\circ}\text{C})$	$t_{TMA}(\text{s})$	$t_{Ar_1}(\text{s})$	$t_{O_3}(\text{s})$	$t_{Ar_2}(\text{s})$
t_{O_3}	200	200	150	1.5	60	3	60
	200	200	150	1.5	60	5	60
	200	200	150	1.5	60	7	60
	200	200	150	1.5	60	10	60
	200	200	150	1.5	60	15	60
	200	200	150	1.5	60	20	60
	200	200	150	1.5	60	30	60
	200	200	150	1.5	60	50	60
	200	200	150	1.5	60	60	60
	200	200	150	1.5	60	60	60
	200	200	150	1.5	60	90	60

Table B.4 variations in O₃ exposure time

Variation	Pressure(Pa)	O ₃ flow (sccm)	$\vartheta_{\text{Substrate}}(^{\circ}\text{C})$	$t_{TMA}(\text{s})$	$t_{Ar_1}(\text{s})$	$t_{O_3}(\text{s})$	$t_{Ar_2}(\text{s})$
t_{Ar_2}	200	200	150	1.5	60	60	3
	200	200	150	1.5	60	60	5
	200	200	150	1.5	60	60	7
	200	200	150	1.5	60	60	10
	200	200	150	1.5	60	60	15
	200	200	150	1.5	60	60	20
	200	200	150	1.5	60	60	25
	200	200	150	1.5	60	60	30
	200	200	150	1.5	60	60	40
	200	200	150	1.5	60	60	50
	200	200	150	1.5	60	60	60
	200	200	150	1.5	60	60	90

Table B.5 variations in Ar purge time after O₃ exposure